JCI The Journal of Clinical Investigation

BIN2 orchestrates platelet calcium signaling in thrombosis and thrombo-inflammation

Julia Volz, … , Markus Sauer, Bernhard Nieswandt

J Clin Invest. 2020. https://doi.org/10.1172/JCI136457.

Research In-Press Preview Cell biology Hematology

Graphical abstract

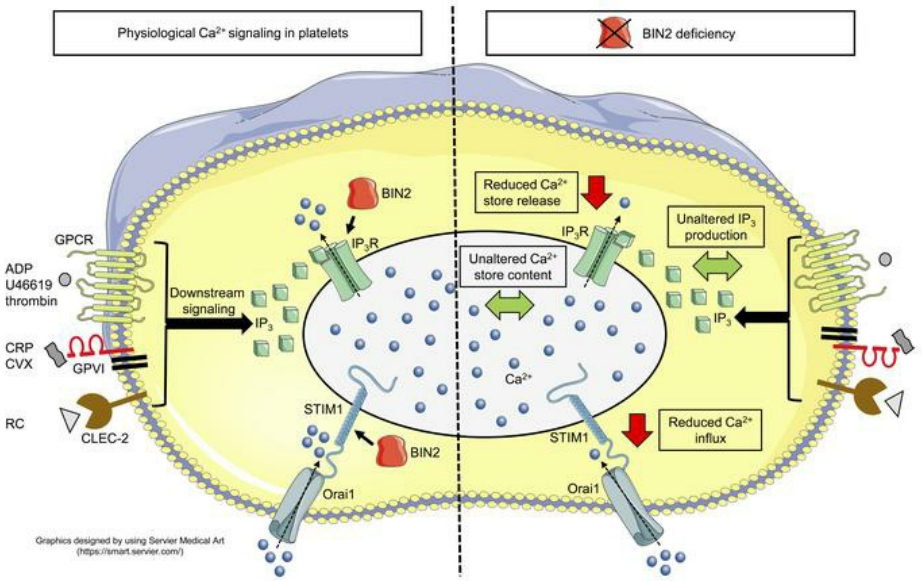

BIN2 orchestrates platelet calcium signaling in thrombosis and thrombo-inflammation

Julia Volz[1,2,*], Charly Kusch[1,2,*], Sarah Beck[1,2], Michael Popp[1,2], Timo Vögtle[1,2], Mara Meub[3], Inga Scheller[1,2], Hannah S. Heil[2], Julia Preu[1,2], Michael K. Schuhmann[4], Katherina Hemmen[2], Thomas Premsler[5], Albert Sickmann[5,6,7], Katrin G. Heinze[2], David Stegner[1,2], Guido Stoll[4], Attila Braun[1,2], Markus Sauer[3], Bernhard Nieswandt[1,2]

[1]Institute of Experimental Biomedicine I, University Hospital Würzburg, Germany

[2]Rudolf Virchow Center, University of Würzburg, Germany

[3]Department of Biotechnology and Biophysics, Biocenter, University of Würzburg, Germany

[4]Department of Neurology, University Hospital Würzburg, Germany

[5]Leibniz-Institut für Analytische Wissenschaften – ISAS – e.V., Dortmund, Germany

[6]Medizinisches Proteom-Center, Ruhr-University Bochum, Bochum, Germany

[7]Department of Chemistry, College of Physical Sciences, University of Aberdeen, United Kingdom

* these authors contributed equally

Attila Braun: present address is Walther-Straub Institute of Pharmacology and Toxicology, Ludwig-Maximilians-Universität München, Munich, Germany

Conflict of interest statement

The authors have declared that no conflict of interest exists.

Word count:

total: 7717 abstract: 162

Address correspondence to:

Bernhard Nieswandt, PhD (Orcid: 0000-0003-1454-7413)

Institute of Experimental Biomedicine I, University Hospital Würzburg and Rudolf Virchow Center, University of Würzburg, Josef-Schneider-Str. 2, 97080 Würzburg, Germany, Phone: + 49 931 31 80405; Fax: + 49 931 201 61652; bernhard.nieswandt@virchow.uni-wuerzburg.de

Abstract

Store-operated calcium entry (SOCE) is the major route of Ca^{2+} influx in platelets. The Ca^{2+} sensor stromal interaction molecule 1 (STIM1) triggers SOCE by forming puncta structures with the Ca^{2+} channel Orai1 and the inositol trisphosphate receptor (IP_3R), thereby linking the endo-/sarcoplasmic reticulum to the plasma membrane. Here, we identified the BAR domain superfamily member bridging integrator 2 (BIN2) as an interaction partner of STIM1 and IP_3R in platelets. Deletion of platelet BIN2 (*Bin2*$^{fl/fl,Pf4\text{-}Cre}$ mice) resulted in reduced Ca^{2+} store release and Ca^{2+} influx in response to all tested platelet agonists. These defects were a consequence of impaired IP_3R function in combination with defective STIM1-mediated SOC channel activation, while Ca^{2+} store content and agonist-induced IP_3 production were unaltered. This severely defective Ca^{2+} signaling translated into impaired thrombus formation under flow and a protection of *Bin2*$^{fl/fl,Pf4\text{-}Cre}$ mice in models of arterial thrombosis and stroke. Our results establish BIN2 as a central regulator of platelet activation in thrombosis and thrombo-inflammatory disease settings.

Introduction

Platelet activation and aggregation at the injured vessel wall is essential for primary hemostasis but may also trigger occlusion of diseased vessels resulting in acute ischemia and infarction of vital organs (1). Platelet inhibition is therefore a central strategy for prevention and treatment of myocardial infarction (2) and stroke (3, 4). Platelet activation is triggered by exposed constituents of the vessel wall or surrounding tissue such as collagens and podoplanin, respectively, or soluble mediators such as ADP, thromboxane A_2, and thrombin locally generated by the coagulation cascade (5). These agonists act through two major classes of signaling receptors, namely immunoreceptor tyrosine-based activation motif (ITAM) coupled receptors or G-protein coupled receptors (GPCRs). While these receptors trigger different signaling pathways, they all activate phospholipase (PL) C isoforms and thus production of diacylglycerol (DAG) and inositol 1,4,5-triphosphate (IP_3). IP_3 binds to inositol trisphosphate receptors (IP_3R), thereby inducing the release of Ca^{2+} from the dense tubular system (DTS), which is the platelet equivalent of the endoplasmic reticulum (ER). This store depletion triggers a large Ca^{2+} influx across the plasma membrane (PM), called store-operated Ca^{2+} entry (SOCE), which is the major route of Ca^{2+} influx in platelets (5, 6). Stromal interaction molecule 1 (STIM1) has been identified as the essential Ca^{2+} sensor localized in the DTS membrane, regulating the Ca^{2+} release-activated Ca^{2+} (CRAC) channel Orai1 in the PM of platelets (7-10).

The functional coupling model, developed in other cells than platelets, suggests that STIM1, Orai1 and IP_3R form puncta structures at the ER-PM junctions, where the actual SOCE may then occur (11-17). While this process forms the essential framework for SOCE in virtually all non-excitable cells, several enzymes and adaptor proteins have been identified to be critical regulator of this process (17-20), thereby allowing a cell-specific assembly of Ca^{2+} signaling systems with very different spatial and temporal dynamics (21, 22). To date, STIM1 adaptors in platelets remain to be identified.

BIN proteins constitute a family of adapter proteins characterized by a common N-terminal Bin-Amphiphysin-Rvs (BAR) domain. Diverse cellular functions of this protein family have been

described, including membrane dynamics (23), organization of the actin cytoskeleton (24), cell cycle control (25), as well as tumor suppression (25, 26). Three different BIN isoforms are known: BIN1, BIN2, and BIN3. BIN1 is ubiquitously expressed and has been shown to fold cardiac T-tubules, thereby facilitating cytoskeleton-based Ca^{2+} channel trafficking to the T-tubule membranes and refraining free diffusion of local Ca^{2+} and K^{+} ions (27, 28). The role of BIN3 in cellular processes is barely understood, except for its involvement in the regulation of Rac1- and Cdc42 dependent processes in myogenesis (29). Likewise, only very limited information about the function of BIN2, predominantly found in hematopoietic cells (30), exists. Previous studies showed that BIN2 is present at podosomes of adherent leukocytes indicating a functional role in cell adhesion and possibly integrin activation (31). In addition, siRNA knockdown of BIN2 in macrophages led to enhanced phagocytosis and reduced cell movement of monocytes and mast cells (31).

Here, we used biochemical and proteomic approaches in combination with super-resolution microscopy to identify BIN2 as a highly expressed interaction partner of STIM1 in platelets. Using a MK/platelet-specific knockout (KO) mouse model, we show that BIN2 plays a key role in Ca^{2+} store release and SOCE in platelets by directly or indirectly interacting with two key molecules in Ca^{2+} homeostasis, IP_3R and STIM1. This selective Ca^{2+} signaling defect translated into protection of *Bin2*$^{fl/fl,Pf4\text{-}Cre}$ mice in models of arterial thrombosis and stroke.

Results

STIM1 interacts with BIN2 in platelets

To identify STIM1 binding partners in platelets, we coupled the recombinantly expressed C-tail of human STIM1 (aa 484-685; Suppl. Figure 1A) to an Affi-Gel® 10 matrix affinity column and loaded it with triton X-100 lysed resting human platelets (10 mg per ml affinity support). Loading of equal volumes of pooled platelet lysates on uncoupled Affi-Gel® 10 matrix (without STIM1 C-tail) served as a negative control. Eluted fractions of the affinity columns were resolved by 1D-SDS-PAGE and bands were visualized by subsequent silver staining (Suppl. Figure 1B). Eighteen differential protein bands that were reproducibly detected only in the STIM1 C-tail affinity column samples were excised, tryptically digested, analyzed by nano-LC-ESI-MS/MS and compared against the UniProtKB/Swiss-Prot human subset. By this approach, we identified >25 STIM1 C-tail bound proteins, among them several cytoskeletal proteins (Suppl. Table 1). Following analysis of different hits, we took special interest in the robustly detectable adapter protein bridging integrator 2 (BIN2 - UniProtKB/Swiss-Prot accession number: Q9UBW5-1), given the involvement of BIN1 in Ca^{2+} signaling of cardiomyocytes. In line with previous reports (30), immunoblotting of different human tissues confirmed the restricted expression of BIN2, with the highest expression level detected in platelets (Figure 1A). To confirm the interaction of BIN2 and STIM1, we performed an immunopreciptitation with an anti-BIN2 antibody in human platelet lysate. We could demonstrate the presence of STIM1 in the pulldown after BIN2 precipitation by western blot analysis (Figure 1B) and silver staining of the SDS page (Suppl. Figure1C). Furthermore, we incubated the GST-tagged STIM1 C-tail with recombinantly expressed BIN2 protein and performed a pulldown for GST. Using SDS-PAGE and silver staining we detected both, the GST-tagged STIM1 (~50 kDa), but also BIN2 (~70 kDa), demonstrating a direct interaction between the two proteins (Figure 1 C). The rather small amount of BIN2 precipitated in this experiment indicates a weak interaction of the two proteins, which is also reflected by a dissociation constant (K_d) of ~ 196 µM, as determined in a fluorescence polarization assay, where increasing amounts of BIN2 were titrated against

labeled STIM1. The shallow curve with a hill slope of < 1 indicates a more complex binding mode, such as negative cooperativity, rather than a simple one-site binding (Suppl. Figure 2).

BIN2-deficient mice are viable and fertile

In accordance with the expression pattern in humans, BIN2 expression in mouse tissue was also largely restricted to hematopoietic cells with the highest levels detectable in platelets (Figure 1D). The interaction between STIM1 and BIN2 was confirmed in mouse platelet lysates by immunoprecipitation of BIN2, and subsequent detection of STIM1 (Suppl. Figure 1D,E).

To assess the function of BIN2 in vivo, we generated a constitutive knockout mouse strain (*Bin2*$^{fl/fl,CMV\text{-}Cre}$, referred to as *Bin2*$^{-/-}$). Homozygous *Bin2*$^{-/-}$ mice were born at a normal Mendelian ratio, viable, fertile and appeared healthy, indicating that BIN2, in contrast to STIM1 (9, 32) or Orai1 (10, 33), is dispensable for embryonic development. Western blot analysis confirmed the complete loss of BIN2 expression in all tested tissues (Figure 1D). Basic blood parameters, including platelet count and size were not altered in *Bin2*$^{-/-}$ mice as compared to *WT* littermates (Suppl. Table 2).

To circumvent potential indirect effects of global BIN2 deficiency on platelet function, we used Pf4-Cre transgenic mice to generate a platelet/megakaryocyte specific BIN2 KO mouse line (*Bin2*$^{fl/fl,Pf4Cre}$). The absence of BIN2 protein in platelets of *Bin2*$^{fl/fl,Pf4\text{-}Cre}$ mice was confirmed by Western blotting (Figure 2A). The basic blood parameters including platelet count, size, as well as the platelet ultrastructure and lifespan were unaltered as compared to the respective littermate control (Suppl. Table 3; Suppl. Figure 3A,B). Investigations of cryosections of the bone marrow of *Bin2*$^{fl/fl,Pf4\text{-}Cre}$ mice revealed no difference in megakaryocyte morphology and number (Suppl. Figure 3C). Of note, expression levels of glycoprotein (GP) V, GPVI as well as integrin β1 and CD9 were slightly reduced in *Bin2*$^{fl/fl,Pf4\text{-}Cre}$ platelets compared to *WT* control (Suppl. Figure 3D).

Diminished Ca^{2+} responses in *Bin2*$^{fl/fl,Pf4\text{-}Cre}$ platelets

Given the interaction between STIM1 and BIN2, we investigated the role of BIN2 in platelet Ca^{2+} homeostasis. We found comparable Ca^{2+} store content in *Bin2*$^{fl/fl,Pf4\text{-}Cre}$ and *Bin2*$^{fl/fl}$ littermate (*WT*) platelets, as measured by treatment of the cells with ionomycin in the absence of extracellular Ca^{2+} (*WT*: 344.2 ± 104 nM; *Bin2*$^{fl/fl,Pf4\text{-}Cre}$: 316.2 ± 55.25 nM) (Figure 2B; Suppl. Figure 4). Also the Ca^{2+} store release evoked by the sarcoplasmic/ER Ca^{2+} ATPase (SERCA) pump inhibitor thapsigargin (TG) was indistinguishable between the two groups (*WT*: 73.75 ± 14.89 nM; *Bin2*$^{fl/fl,Pf4\text{-}Cre}$: 83.78 ± 15.48 nM) (Figure 2C; Suppl. Figure 4). This is in line with the normal Ca^{2+} store content in Orai1 deficient platelets (10), but in contrast to STIM1 deficiency, where a reduced Ca^{2+} store content in platelets was observed (9) which points towards a role of STIM1 in Ca^{2+} store filling, which is independent of BIN2. Remarkably, however, the TG-evoked Ca^{2+} influx in the presence of extracellular Ca^{2+} was diminished in the absence of BIN2 (*WT*: 877.5 ± 391.2 nM; *Bin2*$^{fl/fl,Pf4\text{-}Cre}$: 264.6 ± 143.6 nM) (Figure 2D; Suppl. Figure 4), suggesting a defect in the STIM1-dependent opening of Orai1 channels. Next, we studied receptor-dependent Ca^{2+} responses to GPCR agonists (ADP, thrombin and the stable TxA_2 analogue U46619) and (hem)ITAM-dependent agonists, acting on GPVI (collagen-related peptide, CRP and convulxin, CVX) or CLEC-2 (rhodocytin, RC). Interestingly, Ca^{2+} store release was significantly reduced in response to all tested agonists (Figure 2E; Suppl. Figure 5). In line with these findings and the results from the TG experiments, SOCE was also diminished in the mutant platelets, resulting in an overall severely defective Ca^{2+} response (Figure 2F; Suppl. Figure 5). Together, these results clearly demonstrated a critical role of BIN2 in STIM1/Orai1-mediated SOCE, but also in agonist-induced Ca^{2+} store release. Of note, STIM1 expression levels were unaltered in *Bin2*$^{fl/fl,Pf4\text{-}Cre}$ platelets (Figure 2G).

Defective IP_3R function in *Bin2*$^{fl/fl,Pf4\text{-}Cre}$ platelets

In order to identify the mechanisms underlying the defective agonist-induced Ca^{2+} store release, we analyzed the signal transduction pathways downstream of the (hem)ITAM receptors GPVI and CLEC-2. The phosphorylation of the key signaling molecules Syk

(Y519/520), LAT (Y191) and PLCγ2 (Y753) were unaltered in response to the GPVI agonist CVX or the CLEC-2 agonist RC (Figure 3A,B). A central downstream pathway of all agonists is the PLC-dependent hydrolysis of PIP_2 into DAG and IP_3. In line with the unaltered (hem)ITAM tyrosine phosphorylation cascade, the amount of IP_3 produced by *Bin2*$^{fl/fl,Pf4\text{-}Cre}$ platelets upon activation with CVX or RC was indistinguishable from *WT* controls (Figure 3C). This was also the case for the GPCR agonist thrombin suggesting that the defect was located downstream of IP_3 generation. We therefore analyzed IP_3R expression levels in the mutant platelets but found them to be unaltered compared to *WT* controls (Figure 3D). To assess the functionality of the IP_3R, we loaded platelets with inactive caged IP_3, which can be activated with an UV-light pulse during the measurement (34). Strikingly, in these experiments both, Ca^{2+} store release as well as SOCE, were significantly reduced in *Bin2*$^{fl/fl,Pf4\text{-}Cre}$ platelets compared to *WT* controls (Figure 3 E,F; Suppl. Figure 5), strongly suggesting a functional defect of the IP_3Rs in mutant platelets.

BIN2 interacts with STIM1 and IP_3R

The results above indicated that BIN2 may not only interact with STIM1 but possibly also with IP_3Rs to regulate Ca^{2+} signaling in platelets. To test this hypothesis directly, we performed a pulldown assay, where we incubated *Bin2*$^{fl/fl,Pf4\text{-}Cre}$ platelet lysates with recombinant His-tagged BIN2. Following purification with NI-NTA beads, the different fractions were eluted and analyzed by immunoblotting. A high amount of BIN2 was detected in the eluate fractions (Figure 3G), demonstrating the functionality of the pulldown. Furthermore, STIM1 was robustly detected in the eluate fractions (Figure 3G), confirming the results obtained with human platelets (Figure 1B). In addition, we also identified IP_3R in the eluate fraction of the pulldown, demonstrating a robust direct or indirect interaction of BIN2 with both, STIM1 and IP_3R in platelets. To ensure specificity, we screened for the unrelated protein RhoA, which was absent in the eluate fractions (Suppl. Figure 6A) and performed silver staining of the SDS page to visualize total protein content (Suppl. Figure 6B).

To investigate the localization of BIN2 in murine platelets, we used super-resolution microscopy by *direct* stochastic optical reconstruction microscopy (*d*STORM)(35, 36) in combination with a newly in-house generated monoclonal anti-mouse BIN2 antibody. Resting platelets were immobilized on glycine, whereas thrombin-activated platelets were allowed to spread on fibrinogen, previous to the staining procedure. An inhomogeneous distribution of BIN2 in the cytoplasm was detected in resting *WT* platelets, whereas no staining was observed in *Bin2*$^{fl/fl,Pf4\text{-}Cre}$ platelets (Figure 4A). In spread *WT* platelets, BIN2 was mainly located to the cell center, with multiple sites of clustering (Figure 4B). These results indicated accumulation of BIN2 at internal membranes.

In human platelets, dual-color *d*STORM imaging allowed us to visualize the distribution of BIN2 and STIM1 in resting platelets on glycin and thrombin activated spread platelets on fibrinogen (Figure 4 C,D). A neighbor density analysis of the distance dependent BIN2 density around STIM1 localization events confirmed the accumulation of BIN2 in close vicinity to STIM1 (Figure 4 E-G & Suppl. Figure 7). Most notable, an increased BIN2 density was consistently found at distinct distances of ~50 and ~100 nm (see light gray highlighted areas in Figure 4 F,G) for both activated and resting platelets. These findings strongly suggest co-localization hotspots of STIM1 and BIN2 in human platelets. The exact molecular constellation of the STIM1/BIN2 interaction, however, could not be resolved due to large size of IgG antibodies of ~10-15 nm (37). Note that comparative co-localization studies in mouse platelets were not possible due to the lack of functional *d*STORM antibodies for mouse STIM1.

Defective activation responses in *Bin2*$^{fl/fl,Pf4\text{-}Cre}$ platelets

The above results had shown a severe Ca^{2+} signaling defect in *Bin2*$^{fl/fl,Pf4\text{-}Cre}$ platelets. To evaluate the functional consequences of the observed Ca^{2+} defect on the activation of *Bin2*$^{fl/fl,Pf4\text{-}Cre}$ platelets, we performed flow cytometric analysis of agonist-induced integrin αIIbβ3 activation and P-selectin surface exposure, a marker of α-granule release (Figure 5A,B). Activation of *Bin2*$^{fl/fl,Pf4\text{-}Cre}$ platelets was largely unaltered in response to the GPCR agonists ADP, thrombin and U46619 with exception of a weak but significant reduction upon co-

stimulation with U46619 and ADP. However, the response of *Bin2*$^{fl/fl,Pf4\text{-}Cre}$ platelets towards the GPVI agonists CRP or CVX was significantly reduced compared to *WT* controls. Similar observations were made upon stimulation with the CLEC-2 agonist rhodocytin (Fig 5A,B). In line with the decreased integrin activation, aggregation responses to (hem)ITAM-specific stimulation were reduced, which was most evident at low agonist concentrations (Figure 5C). No differences in aggregation upon stimulation with the GPCR agonists thrombin, ADP and U46619 or the combination of ADP/U46619 were detected (Figure 5C, Suppl. Fig 6C). These results are in accordance with previous studies showing that also the Ca^{2+} defects observed in STIM1 and Orai1 deficient platelets are of particular functional relevance for (hem)ITAM-mediated but to a much lesser extent for GPCR-mediated activation responses under static conditions (8-10). Since Ca^{2+} and SOCE are of particular importance for phosphatidylserine (PS)-exposure upon platelet activation, we investigated this process by measuring the ability of *Bin2*$^{fl/fl,Pf4\text{-}Cre}$ platelets to bind AnnexinA5 in flow cytometry. We found significantly reduced PS-exposure in response to the tested agonists in the mutant platelets compared to *WT* control (Figure 5D). Of note, *Bin2*$^{fl/fl,Pf4\text{-}Cre}$ platelets showed unaltered spreading on fibrinogen, indicating that BIN2 is neither required for integrin αIIbβ3 outside-in signaling nor for the rapid rearrangements of the actin cytoskeleton that are underlying this process (Suppl. Figure 6D) (38). This is in line with normal shape change observed in aggregometry (Figure 5C) and unaltered ultrastructure (Suppl. Figure 3B).

Thrombus formation at sites of vascular injury requires stable shear-resistant platelet adhesion on the extracellular matrix and auto- and paracrine platelet activation by locally released secondary mediators. When whole blood was perfused over immobilized collagen at a shear rate of 1700 s^{-1}, *WT* platelets adhered rapidly to the collagen-coated surface and recruited additional platelets, resulting in the formation of stable three-dimensional aggregates. In sharp contrast, adhesion and aggregate formation of *Bin2*$^{fl/fl,Pf4\text{-}Cre}$ platelets was severely impaired, resulting in a 65 % and 75 % reduction in surface coverage and thrombus volume, respectively (Figure 6A). This is in line with the observations made with STIM1 and Orai1 deficient platelets and underlines the importance of Ca^{2+} signaling in platelets under shear flow conditions (39).

Furtheremore, the reduced PS-exposure of *Bin2*$^{fl/fl,Pf4\text{-}Cre}$ platelets was also confirmed in this experimental setting (Suppl. Figure 6E).

In summary, these results demonstrated impaired integrin activation, degranulation and aggregation of *Bin2*$^{fl/fl,Pf4\text{-}Cre}$ platelets in response to (hem)ITAM agonists under static conditions and defective shear-resistant aggregate formation under flow in vitro.

Impaired hemostasis, defective arterial thrombus formation and reduced thrombo-inflammatory brain infarction in *Bin2*$^{fl/fl,Pf4\text{-}Cre}$ mice

To examine to which extent the observed defects in Ca^{2+} homeostasis of *Bin2*$^{fl/fl,Pf4\text{-}Cre}$ platelets influenced hemostasis, we performed a tail-bleeding assay. Here, a 2 mm segment of the tail tip is cut off with a scalpel and the time until bleeding ceases is determined. No differences between *Bin2*$^{fl/fl,Pf4\text{-}Cre}$ and *WT* mice were observed (Figure 6B), confirming the previous finding that even severely impaired Ca^{2+} signaling in platelets does per se not cause a major hemostatic defect (8-10).

Next, we investigated occlusive thrombus formation in the abdominal aorta following mechanical injury of the vessel by compression with a forceps. The time to vessel occlusion was significantly prolonged in *Bin2*$^{fl/fl,Pf4\text{-}Cre}$ mice as compared to *WT* mice and 3 out of 14 vessels did not occlude during the observation time of 30 minutes (mean occlusion time: *WT*: 230 ± 85 seconds; *Bin2*$^{fl/fl,Pf4\text{-}Cre}$: 323 ± 90 seconds; P = 0.012; Figure 6C). It has been shown that defective GPVI signaling can be partially compensated for by TxA_2-mediated G_q/G_{13}-induced signaling pathways, which enables platelets to further deplete the Ca^{2+} stores and to enhance SOCE (40-42). Therefore, we investigated the role of TxA_2-induced signaling in vivo by inhibiting TxA_2 synthesis in *WT* and *Bin2*$^{fl/fl,Pf4\text{-}Cre}$ mice by intravenous administration of a low dose of acetylsalicylic acid (ASA: 1 mg/kg bodyweight) and subsequently assessed tail bleeding times and occlusive thrombus formation in the injured aorta. ASA treatment had no major effect in *WT* mice, but resulted in significantly prolonged tail bleeding times in *Bin2*$^{fl/f,Pf4Cre}$ mice (Figure 6B). Similarly, ASA-treated *WT* mice developed occlusive thrombi in the

mechanically injured aorta, whereas only 4 out of 14 vessels in ASA-treated *Bin2*$^{fl/fl,Pf4\text{-}Cre}$ mice occluded (P = 0.0002; Figure 6D). Together, these data confirm that functional defect in (hem)ITAM dependent platelet activation can be partially compensated for by TxA_2-induced signaling pathways under in vivo conditions.

Platelets are increasingly recognized as key modulators of inflammatory responses and their concerted action with components of the immune system to cause tissue damage is referred to as thrombo-inflammation. This was first described in the setting of (experimental) stroke, where platelets and T cells drive secondary thrombo-inflammatory brain infarct growth despite successful recanalization of the previously occluded brain artery. Recent experimental data has highlighted a critical role of the platelet GPVI-LAT-PLCγ2-STIM1/Orai1 axis in this process (9, 10, 43) and increased expression levels of STIM1/Orai1 have been proposed to serve as a predictor for poor outcome of stroke (44). To assess the pathophysiological significance of BIN2-dependent SOCE in this process, we subjected *Bin2*$^{fl/fl,Pf4\text{-}Cre}$ mice to the transient middle cerebral artery occlusion (tMCAO) model of ischemic stroke, in which the middle cerebral artery (MCA) is transiently occluded by insertion of a filament as described previously (45). After removal of the filament, the animals were monitored for another 24 hours before the infarct sizes were assessed quantitatively on 2,3,5-triphenyltetrazolium chloride (TTC)–stained brain slices (Figure 6E). In *Bin2*$^{fl/fl,Pf4\text{-}Cre}$ mice, infarct volumes were reduced by >30% compared to control mice (*WT*: 90±6 mm^3, *Bin2*$^{fl/fl,Pf4\text{-}Cre}$: 59±7 mm^3; P=0.003; Figure 6F). The number of occluded vessels in the ipsilateral hemisphere, indicative of tissue damage and resultant thrombotic activity, as well as the number of accumulated neutrophils and $CD11b^+$ cells were reduced in the ipsilateral hemispheres of *Bin2*$^{fl/fl,Pf4\text{-}Cre}$ mice as compared to *WT* littermates (Figure 6G-I). In summary, these results demonstrated that BIN2 deficiency in platelets results in defective thrombus formation under flow and provides profound protection against arterial thrombosis and amelioration of thrombo-inflammatory brain infarction.

Discussion

This study is, to our knowledge, the first to describe an adapter protein that regulates both, IP_3R and STIM1 function in platelets, thereby connecting Ca^{2+} store release and SOCE function. Our data demonstrates a direct interaction of BIN2 with STIM1, however, the weak binding affinity and the more robust interaction of the proteins in cell lysates strongly suggests that this interaction is stabilized by additional binding partners in a multi-protein complex at the Ca^{2+} stores.

First evidence that the IP_3R can modify Ca^{2+} influx not only indirectly by releasing Ca^{2+} from the internal store but also by a direct effect on major regulators of Ca^{2+} entry was its reported interaction with transient receptor potential (TRP) channels in HEK cells (46). Conversely, another study revealed a regulating effect of STIM1 on the activity of IP_3R by direct interaction of both proteins in bovine aortic endothelial cells (47). Also, in STIM1 KO, but not in ORAI1 KO platelets a reduced store release was detected in response to all tested agonists (9, 10) - however, the diminished store content in these platelets made a direct conclusion on the functional influence of STIM1 on IP_3R difficult. Furthermore, immobile IP_3R clusters, responsible for the Ca^{2+} release from the ER, co-localize with STIM1 puncta that form upon activation of SOCE (16). The association of IP_3R to STIM1 has been shown to provide a reduced calcium microenvironment near the STIM1 EF-hand, its calcium sensing part residing inside the Ca^{2+} store, thereby facilitating puncta formation and enhancing Orai1 activation and SOCE (17). Based on the data presented here, it is tempting to speculate that BIN2 may be involved in the formation of these IP_3R-STIM1 complexes. Of note, the IP_3R was not detectable in immunoprecipitation experiments neither with human nor with mouse platelet lysate (data not shown). This might be a consequence of the low amount of BIN2 protein precipitated in the IP experiments as compared to concentration of recombinant BIN2 in pulldown experiments. Alternatively, BIN2 might regulate IP_3R function independently of direct or indirect physical interactions with the receptor, e.g. by modulating the complex upstream regulatory signaling pathways which control IP_3R function. These include small molecules, such as nucleotides as

well as protein kinases and phosphatases (48, 49). Further studies will be required to unravel the exact underlying molecular mechanisms.

Super-resolution microscopy data also support the BIN2-STIM1 interaction. Particularly, our neighbor density analysis (50) revealed an accumulation of BIN2 in close vicinity to STIM1 at characteristic distance regions of 50 and 100 nm (for both activated and resting human platelets). These findings strongly suggest co-localization hotspots of STIM1 and BIN2 that have not been described before. Such hotspots may form due to steric hinderance induced by the large size of IgG antibodies used in immunolabeling (37). It is likely that the 50 nm pattern represents the minimal possible distance with the width of each peak mostly indicating the flexibility of the linkers.

Of note, Ambily *et al.* (51) have previously performed immunoprecipitation of STIM1 protein from thapsigargin-treated human platelet lysates and identified four potential interaction partners, which did, however, not include BIN2. This rather low number of proteins identified might be a consequence of lower sensitivity by precipitating limited amounts of endogenous STIM1 protein with an antibody. Of the four molecules identified in their study, Mysosin-9 and actin also yielded high scores in our experiments; however, we did not identify DOCK10 or Thrombospondin. This might be explained by methodological differences, e.g. by the use of a truncated STIM1-construct in our study or the thapsigargin-pretreatment of platelets in the study of Ambily *et al*..

Interestingly, BIN1, another member of the BIN protein family, has recently been identified to regulate the microtubule-mediated transport and surface expression of the calcium channel Cav1.2. in cardiomyocytes (27). Cardiomyocyte-specific loss of BIN1 results in a decreased number of protective membrane folds of T-tubules and alters cation diffusion within the T-tubules, thus increasing the duration of action potentials (28). Of note, we found that the ultrastructure, as well as the ability to change the morphology during spreading was not altered in BIN2-deficient platelets (Suppl. Figure 3B, 6D), indicating that BIN2 exerts its effect on Ca^{2+} signaling via a different mechanism. As previously described for mice lacking STIM1 (9) or

Orai1 (10), the severe SOCE defect in *Bin2*$^{fl/fl,Pf4\text{-}Cre}$ platelets hardly affected their functional responses to GPCR agonists, but impaired cellular activation through (hem)ITAM signaling. The difference in SOCE dependence between these two major activation pathways is currently not understood but may be related to different kinetics in IP_3 production, since the (hem)ITAM/PLCγ2-axis responds slower to a stimulus compared to the GPCR/PLCβ signaling.

Of note, we have also observed a slightly decreased expression of some surface glycoprotein receptors on *Bin2*$^{fl/fl,Pf4\text{-}Cre}$ platelets. Since these alterations were very minor we consider it very unlikely that they significantly contribute to the observed platelet-related phenotype of Bin2 KO mice.

The viability of the *Bin2*$^{-/-}$ animals as well as the unaltered blood parameters demonstrates that BIN2 is dispensable for embryonic development. This is in contrast to STIM1 and Orai1 mutant animals which die perinatally (8-10, 32), indicating that these molecules may not be suitable pharmacological targets for long-term treatment of thrombotic diseases, due to undesired effects on different tissues, including immune cells and skeletal muscle, which are also observed in patients with STIM1 or ORAI1 mutations (52). The more restricted expression of BIN2 in the hematopoietic system and its central role in Ca^{2+} signaling in platelets provides proof of principle that the adaptors involved in Ca^{2+} signaling vary between different cell types and might thereby be good targets to selectively inhibit or modulate the Ca^{2+} signaling machinery in a cell type-selective cell manner. Remarkably, platelet-specific BIN2 deficiency significantly reduced cerebral infarct growth in a model of acute ischemic stroke without increasing the risk of intracranial hemorrhage. Although further studies will be required to assess the druggability of BIN2, our findings corroborate the concept that molecules modulating Ca^{2+} homeostasis specifically in platelets may become promising novel targets for the prevention and/or treatment of thrombotic and thrombo-inflammatory diseases with minimal effects on normal hemostasis.

Methods

Animals

Generation of *Bin2*$^{fl/fl}$ mice: A 9.96 kb region used to construct the targeting vector was designed such that the 5' homology arm extends about 2.83 Kb 5' to the 3' end of the LoxP-FRT flanked Neo cassette. The 3' homology arm ends 3' to single LoxP cassette and is 6.52 Kb long. The LoxP-FRT flanked Neo cassette was inserted 403 bp upstream of exon 3. The single LoxP site was inserted 157 bp downstream of exon 3. DNA of the targeting vector was linearized by NotI digestion and then transfected by electroporation of BA1 (C57Bl/6 x 129/SvEv) (Hybrid) embryonic stem cells. After selection with G418, surviving clones were expanded for PCR analysis. 5 positive clones were identified and expanded. Targeted iTL BA1 (C57BL/6N x 129/SvEv) hybrid embryonic stem cells were microinjected into blastocysts of pseudo-pregnant C57BL/6 females. Highly chimeric offspring was mated to C57BL/6 FLP mice to remove the Neo cassette and backcrossed to C57BL/6 females resulting in *Bin2*$^{fl/+}$ mice. Constitutive knockout mice and MK-/platelet-specific knockout mice were generated by mating with CMV-cre or PF4-cre mice, respectively (53, 54). Intercrossing of the respective offspring resulted in *Bin2*$^{fl/fl,CMV\text{-}Cre+/-}$ (referred to as: *Bin2*$^{-/-}$) mice or *Bin2*$^{fl/fl,PF4\text{-}Cre+/-}$ mice, respectively. *Bin2*$^{fl/fl,PF4\text{-}Cre-/-}$ littermates served as controls.

Transformation of competent *E. coli* cells

For transformation, chemically competent *E. coli* BL21 (DE3) or *E. coli* BL21 (DE3) pRARE2 cells were incubated with 50 ng plasmid DNA of *stim1* C-tail (aa 484-685; Suppl. Figure 1A) in pGEX6p1 or *bin2* in pETM11, respectively, for 30 min on ice. Transformation was triggered by a 45 s heat shock at 42°C with subsequent incubation for 3 min on ice. Thereafter, bacteria were supplied with 500 µl LB-medium and incubated at 450 rpm for 1.5 h at 37°C. Positive clones were selected by plating the transformation mixture on LB-agar plates (10 g/l Bacto tryptone, 5 g/l Bacto yeast extract, 5 g/l NaCl) containing the respective antibiotics (50 µg/ml Amp and 34 µg/ml Cam for *stim1* C-tail in pGEX6p1 or 50 µg/ml Kan for *bin2* in pETM11 and 34 µg/ml Cam) and incubated overnight at 37°C.

Protein production

A single colony was used to inoculate 25 ml LB (for *stim1* C-tail in pGEX6p1) or 100 ml TB (12 g/l tryptone, 24 g/l yeast extract, 4 ml/l glycerol, 0.017 M KH_2PO_4, 0.072 M K_2HPO_4) medium (for *bin2* in pETM11) containing antibiotics at 37°C and 200 rpm overnight. The next day, these pre-cultures were used to inoculate 2.5 l LB or 2 l TB medium supplemented with antibiotics and cultivated at 37°C and 200 rpm until bacterial concentration reached an OD_{600} of 0.4-0.6. Protein expression was induced by addition of IPTG (0.5 mM). Bacterial cultivation was subsequently continued at 16°C and 200 rpm for 16-24 hours (for *stim1* C-tail in pGEX6p1) or 2 h (for *bin2* in pETM11). Cells were harvested by centrifugation at 6,000 rpm for 15 min at 4°C (Beckman Coulter centrifuge, Rotor type JA-10) and cell pellets (up to 20 g/ 500 ml expression culture) were flash-frozen and stored at -80°C. Generally, protein production was controlled by 1D-SDS-PAGE and Western blotting.

Protein purification

STIM1 C-tail: The harvested cell pellets were resuspended in chilled lysis buffer (50 mM Tris-HCl, 150 mM NaCl, pH 8, supplemented with protease- and phosphatase inhibitors) to a final concentration of 0.2 g/ml. Subsequent cell lysis was performed by sonification (4 x 30 sec) on ice. The cell lysate was centrifuged at 16,000 rpm for 1 h at 4°C (Beckman Coulter centrifuge, Rotor type JA 25.50) and the resulting supernatant was incubated with Ni-NTA agarose (0.5 ml per 1 g starting material, pre-equilibrated with lysis buffer) under constant stirring for 1 h at 4°C. Following incubation, the Ni-NTA agarose was transferred to an Econo-Column® 2.5x 20 cm column body (Bio-Rad Laboratories), washed intensively with at least 150 mL lysis buffer before the bound protein was eluted with 25 mL lysis buffer supplemented with elution buffer (50 mM Tris-HCl, 150 mM NaCl, pH 8, supplemented with 250 mM Imidazol). The protein was concentrated using Amicon Ultra® centrifugal filter units to a volume of 1 mL and further purified using size exclusion chromatography with a Superdex 200 Increase 10/300 GL column pre-equilibrated with FPLC buffer (50 mM Tris-HCl, 150 mM NaCl, pH 8.0) on an Äkta pure 25 system (GE Healthcare). Fractions were collected (1 ml volume per fraction) and stored at 4°C.

Success of the purification was verified using 1D-SDS-PAGE and Western blotting. Afterwards fractions containing the pure protein were pooled, concentrated using Amicon Ultra® centrifugal filter units and protein concentration was determined using a NanoDrop™ device (Thermo Scientific). The protein was stored at -80°C until further usage.

BIN2: The harvested cell pellets were resuspended in buffer A (50 mM HEPES, 150 mM NaCl, 5% Glycerol, pH 7.6; 10 ml per g pellet). To separate the soluble and insoluble protein fraction, cells were lysed mechanically by sonification (4 x 30 sec) on ice. The cell lysate was centrifuged at 16,000 rpm for 1 h at 4°C (Beckman Coulter centrifuge, Rotor type JA 25.50). The supernatant was subsequently subjected to Immobilized Metal Affinity Chromatography (IMAC) on a FPLC system (Äkta pure 25 M, GE Healthcare) with an attached HisTrap HP 5 ml column (GE Healthcare). The sample was loaded completely onto the column, which was pre-equilibrated in buffer A, then the column was washed with 20 CV buffer A. Two washing steps with 5 % and 12 % of Buffer B, (50 mM HEPES, 150 mM NaCl, 5% Glycerol, 400 mM Imidazole, pH 7.6) respectively. Proteins were eluted using 100% elution buffer B. Samples of all purification steps were analyzed by SDS-PAGE, and the eluate fractions that contained the target protein were pooled. The purified protein was concentrated using Amicon Ultra® centrifugal filter units and protein concentration was determined using a NanoDrop™ device (Thermo Scientific). In general, the purified proteins were flash-frozen and stored until further usage at -80°C and the purification procedure was monitored by 1D-SDS-PAGE and Western blotting.

GST Pulldown Assay

To determine whether the interaction between BIN2 and STIM1 is direct, GST pulldown assays with purified recombinant proteins were performed. For this purpose, 2.5 µM GST-tagged STIM1 C-tail in 200 µl Pulldown buffer (1x PBS supplemented with 5 mM DTT) were coupled to 20 µl preequilibrated Pierce™ Glutathione Agarose beads for 2 h at 4°C under constant rotation. Afterwards, the beads were washed 3 times with 400 µl pulldown buffer (centrifugation 500 g, 1 min, 4°C). Subsequently, increasing concentrations of recombinant BIN2 (starting with

2.5 µM up to 500 µM) in 200 µl Pulldown buffer were incubated with the agarose beads for 2 h at 4°C under constant rotation. Afterwards, the beads were washed 3 times with 400 µl pulldown buffer (centrifugation 500 g, 1 min, 4°C), supplemented with 5 µl 4x Laemmli buffer and samples were analysed by silverstaining.

Immobilization of purified recombinant STIM1 C-tail on Affi-Gel 10

Protein coupling to Affi-Gel 10 (BioRad Lab GmbH, Munich, Germany) was performed under aqueous conditions according to the manufacturer's instructions. For each sample, an Affi-Gel 10 slurry volume of 1 ml was transferred to a Econo Chromatography Column (2.5 x 20 cm) and washed with 3 CV deionized water (4°C) at gravity flow. Upon addition of the protein solution (at least 0.5 ml per ml gel) binding was performed by head-over-tail rotation at 4°C for 4 hours. The column was subsequently washed with 1 CV PBS (pH 7.4) and remaining free active ester was blocked by incubating in 1 M ethanolamine-HCl solution (pH 8.0, at least 0.1 ml per ml gel) at 4°C for 1h. Finally, the resulting affinity matrix was washed with 3 CV of ice-cold deionized water and stored in an aqueous solution of 0.2% (w/v) sodium azide (pH 7.4) at 4°C.

Interactome screening of native platelet lysates

The generated STIM1 C-tail affinity column was washed twice in ice-cold deionized water and then pre-equilibrated in 10 CV ice-cold PBS (pH 7.4) at 4°C. Native platelet lysate was added (at least 10 mg per ml affinity support), the remaining column volume was filled with platelet lysis buffer and incubation was performed by head-over-tail rotation overnight at 4°C. In parallel, to also evaluate the impact of unspecific protein binding to the affinity column/material, an equal volume of native platelet lysate was incubated with uncoupled Affi-Gel 10 matrix (i.e. control column, Ctrl). The next day, the supernatant was discarded by gravity flow, the bead material was washed with 10 CV PBS and bound proteins were eluted by applying a pH-gradient of 10 mM Glycine/HCl pH 6.0, pH 5.0, pH 4.0, pH 3.0 and pH 2.0. For each pH-step, an elution volume of 3 CV was collected. Immediately after elution, pH-values were adjusted

to pH 7.0 by addition of an appropriate volume of 1M Tris-buffer, and the total volume of the individual pH-fractions was reduced to 1 ml in a SPD 111V Speed Vac (35°C). The resulting elution samples were either processed further or stored at -80°C.

Mass spectrometry (MS) analysis of the STIM1 interactome

1D-SDS-PAGE of elution samples, gel silver staining, tryptic digestion of differential protein spots and sample preparation for subsequent MS analysis was performed as published previously (55). Tryptic peptides were separated on an Ultimate nano-HPLC system (Dionex, Idstein, Germany) as reported (56) and directly eluted into the online ESI ion source of a Qtrap 4000 (Applied Biosystems, Darmstadt, Germany) and an LTQ XL (Thermo Fisher Scientific, Dreieich, Germany) mass analyzer, respectively. Full MS survey scans from 350 to 2,000 m/z were acquired and the three most intense peaks were subjected to collision-induced dissociation MS/MS. Mass spectra were recorded via the Analyst 1.4 (QTrap) and the Xcalibur 2.1.0 (LTQ) operating software including the mascot.dll 1.6b5 (QTrap) and the extract_msn (LTQ) plug-in for conversion of LC-MS raw data into Mascot generic format. Applying the Mascot™ search algorithm for MS/MS spectra (Mascot Daemon 2.2.02 software platform and Mascot server version 2.2.04), the generated data were searched against the UniProtKB/ Swiss-Prot database (www.uniprot.org, 11/2009, human subset), with Mascot parameters being set as published (56). All MS/MS spectra with a minimum Mascot score of 34 (P-value of 0.05) were taken into consideration for further interpretation and were additionally validated manually.

BIN2 Pulldown

Platelet lysates from *Bin2*$^{fl/fl,Pf4Cre}$ mice (approx. 1 x 10^8 platelets in 50 µl) were mixed with 30 µg of BIN2-HIS (9 µM f.c.) for 5 min at RT, followed by a protein purification step using Ni-NTA agarose (Qiagen). Therefore, 40 µl of Ni-NTA Agarose was filled into a spin column and washed with Buffer A. The lysate was incubated with the beads for 10 min before it was slowly centrifuged through the column (500 g). After three washing steps, the bound protein was

eluted using Buffer B. Each fraction was subsequently analyzed using SDS-PAGE and Western blot.

BIN2 Imunoprecipitation

400 µl of platelet lysate ($1x10^6$ platelets/µl) were incubated on Protein GE Sepharose (GEHealthcare), which has been pre-incubated with 3 µg of the indicated BIN2 antibodies, for 2 h at 4°C. After extensive washing, the beads were incubated with western blot sample buffer for 5 min at 95°C, followed by centrifugation. The protein containing supernatant was analysed by Western blot. Used BIN2 antibodies: anti-BIN2 (Proteintech: 14245-1-AB), anti-BIN2 (N-terminal, Abcam: 175482), 12E1 (lab-made, rat IgG2Aκ) and 2C11 (lab-made, rat IgG2A).

Fluorescence Polarisation Assay

Fluorescence polarisation assay was performed to assess the affinity of the STIM1–BIN2 interaction. The GST-tag of the STIM1 C-tail was cut by 3c protease cleavage (67µg 3c protease per 1 mg STIM1 C-tail), and the cleaved tag was captured with glutathione agarose while the cleaved STIM1 C-tail was collected in the eluate. The GST-free STIM1 C-tail protein was labelled with BDP FL NHS-Ester (Lumiprobe) in TBS overnight at 4°C in a ratio of 1.0:0.8, resulting in a degree of labeling of 0.7.

Recombinant BIN2 was added at concentrations ranging from 0 µM – 400 µM to 1 µM STIM1-BDP FL in a 384 well plate (Greiner) and fluorescence polarisation was measured in triplicates on a CLARIOstar (BMG Labtech) platereader (excitation: 482-16 nm; emission: 530-40 nm). Data analysis and curve fitting was performed with Graphpad Prism.

Human platelet purification and lysis

Blood was taken from consenting healthy, drug-free volunteers. Platelets were purified as described previously (57). Platelet pellets (aliquot volume: 100 µL) were suspended in chilled native platelet lysis buffer (100 mM Tris-HCl, 2 mM EDTA, 2% (v/v) Triton X-100, protease- and phosphatase inhibitors (Complete Mini Protease- and PhosSTOP Phosphatase Inhibitor,

Roche)) and lysed by sonication in a Sonorex RK 52 ultrasonic bath (5 sec at 70% maximum power rate, 10 intervals). Each interval was followed by 3 sec of vortexing and chilling on ice. The resulting lysate was cleared from remaining cellular debris by 30 min centrifugation at 20,000 x g (4°C). The protein content of the supernatant was subsequently quantified by BCA assay.

Mouse platelet preparation

Washed platelets were prepared as described (58). Briefly, mice were anesthesized using isoflurane and bled into 300 µl heparin (20 U/ml in TBS, Ratiopharm). The blood was centrifuged twice at 300g for 6 minutes to obtain platelet-rich plasma (PRP). PRP was supplemented with 0.02 U/ml apyrase (A610, Sigma-Aldrich) and 0.1 µg/ml PGI_2 (P6188, Sigma-Aldrich) and platelets were pelleted by centrifugation at 800 g for 5 minutes, washed twice with Tyrodes-HEPES buffer (134 mM NaCl, 0.34 mM Na_2HPO_4, 2.9 mM KCl, 12 mM $NaHCO_3$, 5 mM HEPES, 5 mM glucose, 0.35% BSA, pH 7.4) containing 0.02 U/ml apyrase and 0.1 µg/ml PGI_2. The platelets were allowed to rest for 30 minutes prior to experiments.

Immunoblotting

Western blot analysis was performed as described previously (58). Untreated or activated platelets were lysed at the respective time points, separated by SDS-PAGE and blotted on a PVDF membrane, on which the proteins were detected using anti-BIN2 antibody (Proteintech: 14245-1-AB), anti-STIM1 antibody (Cell Signalling: 4916), anti-IP_3R antibody (Merck-Millipore: 07-1210), anti-RhoA (Cytoskeleton: ARH04) and and-GAPDH (Sigma-Aldrich: G9545). Human protein lysates were purchased from ProSci. Silver staining of the SDS page was perfomed using the SilverQuest Silver Sraining KIT (LifeTechnologies) according to manufacturer´s instructions.

Blood parameter measurements

The blood parameters were measured using a ScilVET analyzer as previously described (59).

Flow cytometry

Flow cytometry to determine glycoprotein expression, integrin activation and P-selectin exposure was performed as previously described (58). In short, heparinized whole blood was diluted 1:20 in Tyrode's-HEPES buffer. For activation studies, the blood samples were washed twice in Tyrode's-HEPES and finally resuspended in Tyrode's-HEPES buffer containing Ca^{2+} prior to agonist addition. The samples were incubated with saturating amounts of fluorophore-conjugated mAbs for 15 min at room temperature, and analyzed on a FACSCalibur (BD Biosciences, Heidelberg, Germany). The reaction was stopped by addition of 500 µL PBS buffer and samples were directly analyzed on a FACSCalibur (BD Biosciences). Platelet life span was conducted as described previously (58).

To measure PS-exposure on the platelet surface, washed platelets (5 x 10^4 platelets/µl) in Tyrode's buffer with 2 mM Ca^{2+} were incubated with the indicated agonists for 15 min at 37°C in the presence of saturating amounts of Dylight 488-coupled annexin-A5 (purified and labeled in our laboratory). The reaction was stopped by addition of 500 µL PBS buffer with 2 mM Ca^{2+}. Analysis was performed on a FACSCalibur.

Aggregometry

Washed platelets were prepared as described previously (58). For aggregometry, washed platelets (160 µl with 1.5 x 10^5 platelets/µl) were analyzed in the absence (thrombin) or presence (all other agonists) of 70 µg/ml human fibrinogen. Light transmission was recorded on a four-channel aggregometer (Fibrintimer; APACT, Hamburg, Germany) for 10 min and expressed in arbitrary units, with buffer representing 100% light transmission

Spreading

Spreading experiments were performed as described previously (58). Briefly, thrombin stimulated platelets were allowed to spread on fibrinogen coated coverslips for the indicated time points. Representative interference contrast images (Zeiss Axiovert 200 inverted

microscope) were acquired and the different spreading phases were determined for quantification.

Platelet lifespan

Platelet life span was measured by injecting 5 µg of Dylight 488-conjugated anti-GPIX derivative. The percentage of circulating labeled platelets was measured daily by flow cytometry using 50 µl whole blood (60).

Intracellular calcium measurements

The measurements were performed as previously described (61). In brief, washed platelets were loaded with 2.5 µM Fura2/AM (Life Technologies: F1221) in the presence of 0.2 µg/ml pluronic F-127 (Life Technologies: P6867) for 30 min at 37°C. After one washing step, they were resuspended in HBSS and the emission was measured at 509 nm under stirring conditions in a fluorimeter (LS55, PerkinElmer) with excitations alternating between 340 nm and 380 nm. After each measurement calibration was performed with Triton X-100 and EGTA.

IP1 ELISA

To determine IP_1 levels, a measure for IP_3 production in platelets, a commercially available ELISA kit (Cisbio) was used. The platelets were purified from mouse blood as described above with the last washing step performed with phosphate-free Tyrode's . The platelet count was adjusted to 700 000 plt/µl using phosphate-free Tyrode's, containing 2 mM Ca^{2+} and 50 mM lithium chloride. After 5 min incubation with indomethacin (10 µM), apyrase (2 U/ml) and EDTA (5 mM), the platelets were activated with the indicated agonist for 15 min, followed by lysis for 30 min at 37°C using the lysis reagent provided with the kit. The ELISA was performed according to the manufacturer's manual.

Flow chamber

Platelet adhesion under flow was measured by perfusing murine whole blood on glass cover slips, coated with 200 µg/ml fibrillar type I collagen (Takeda). The slides were coated o/n at 37°C and then blocked with 1% BSA/PBS for 1 h at RT. Then 700 µl blood mouse blood was collected in 300 µl heparin (20 U/ml in TBS) and the platelets were labeled with a DyLight 488-conjugated anti-GPIX Ig derivate (0.2 µg/ml) for 5 minutes at 37°C. The blood was perfused over the coverslip at a shear rate of 1,700 sec^{-1}. Phase contrast and fluorescent images were aquired using a Leica DMI6000B inverted microscope (63x/1.3 glycerol HCX PL APO objective) equipped with a Leica DFC 360 FX camera and analysed using ImageJ (NIH).

For measurement of procoagulant activity in this setting, experiments were performed as described above, with the used Tyrode's buffer supplemented with additional 5 U/ml heparin to prevent coagulation. To detect PS-exposing platelets, Tyrode's containing 0.25 µg/ml Annexin-A5 Dylight 488 was perfused over the adherent platelets, followed by a washing step before brightfield and fluorescent images were taken. Procoagulant activity was defined as the ratio of surface coverage of PS-exposing platelets to the total surface covered by platelets.

Tail bleeding time and in vivo thrombus formation

Tail bleeding time and in vivo thrombus formation studies in the mechanically injured abdominal aorta were performed as described elsewhere (58).

tMCAO model

tMCAO was performed as described (45). Briefly, a thread was advanced into the middle cerebral artery to inhibit blood flow for 60 min, followed by removal of the filament allowing reperfusion. 24 hours later, infarct sizes were analyzed in brain sections by 2,3,5-triphenyltetrazolium chloride (TTC) staining. Histology and immunohistochemistry were performed according to standard procedures (62). Cryoembedded coronal brain sections (2 mm) were cut into 10 µm-thick slices. Every tenth slice was used for evaluation. The following antibodies were used: monoclonal antibody anti-CD11b (MCA711, Serotec) and anti-Ly-6B

(MCA771G, Bio-Rad). For quantification of occluded microvessels, brain sections were stained with hematoxylin and eosin.

*d*STORM Sample Preparation

Spread platelets on fibrinogen and resting platelets on glycine were fixed with 3% glyoxal solution (63), quenched with 0.1% $NaBH_4$ (ICN Biomedicals), permeabilized with 0.25% Triton-X 100 (Electran) and blocked in a 5% BSA solution in PBS. Murine platelets were stained with Alexa Fluor 647 coupled anti-BIN2-antibody (generated and modified in our laboratory as described previously (64). Antibody specificity was tested in WB, displaying one band in *WT* and no band in $Bin2^{fl/fl,Pf4Cre}$ platelet lysates), human platelets were stained with Alexa Fluor 532 (AF532) coupled anti-BIN2-antibody (Proteintech: 14245-1-AB) and Alexa Fluor 647 (AF647) coupled anti-STIM1-antibody (Santa Cruz Biotechnology: sc-166840).

*d*STORM microscopy

One color *d*STORM samples were imaged on a widefield setup based on an inverted microscope (Olympus IX-71) equipped with an oil immersion objective (60x, NA 1.45; Olympus). The dye was excited with a diode laser at 641 nm at irradiation intensities between 2-10 kW/cm^2 (Cube 640-100C, Coherent). Emission light was separated from the excitation light using a dichroic mirror (ZT 405/514/635rpc, Chroma Technology Corp.), spectrally filtered by a bandpass filter (Em01-R442/514/647-25; Semrock) and projected onto an EMCCD camera chip (iXon DU-897, Andor). Imaging was performed with an exposure time of 20 ms for 15,000 frames in photoswitching buffer containing 100 mM β-mercaptoethylamin, pH 7.4 without oxygen scavenger (35).

Two-color *d*STORM was performed on the same setup described above. AF647 and AF532 were excited with the appropriate laser systems (Genesis MX639 and MX514, Coherent) at irradiation intensities between 2-10 kW/cm^2. Emission light was separated from the excitation light using a dichroic mirror (ZT 405/514/635rpc, Chroma Technology Corp.), spectrally filtered by a bandpass filter (Em01-R442/514/647-25; Semrock), transmitted by a dichroic beam

splitter (ZT 405/514/635rpc, Chroma Technology Corp.) and respective emission filters (Brightline HC 679/41, Brightline HC 582/75, Semrock), before being projected on two EMCCD camera chips (iXon Ultra DU-897, Andor). Imaging was done with an exposure time of 20 ms for 15,000 frames (red dye) and 30,000 frames (green dye) in photoswitching buffer containing 100 mM β-mercaptoethylamin, pH 6.9 as previously described (56). Fluorescent beads (TetraSpeck) were imaged in both channels over the whole ROI to later correct for chromatic abberations. Spread platelets were imaged by total internal reflection fluorescence (TIRF) illumination, resting platelets were measured by epifluorescence (EPI). *d*STORM images were reconstructed using the open source software rapidSTORM 3.3 (65), matrices for chromatic aberration corrections were done with the bUnwarpJ plugin in Fiji (58).

The neighbor analysis was performed with MatLab (Mathworks Inc.) along the neighbor density analysis concepts described by Malkusch et al. (50). For the analysis only the localization data of STIM1 and BIN2 within the region of interest of a single platelet was considered while in the case of activated platelets only the inner platelet region was considered for STIM1 localizations (Figure 4 C,D). The distance dependent BIN2 density was normalized to the total number of STIM1 localizations in the platelet region of interest and the average BIN2 density at distances between 400 and 500 nm. As controls, random distributions of localization data were generated with densities corresponding to the values of the experimental data.

Statistics

Data is represented as mean ± SD. P-values were calculated with the Student's t-test, Mann-Whitney U test or Kruskal-Wallis test followed by Dunn's multiple comparisons post-hoc test, as indicated in the figure legend. In case of frequency analysis of occluded and non-occluded vessels in the aorta injury model, Fisher's exact test was used to compare groups. For statistical analysis, Graph-Pad Prism 6 Software was used. P values <0.05 were considered as statistically significant (*P<0.05, **P<0.01, ***P<0.001).

Study approval

Animal studies were approved by the district government of Lower Franconia (Bezirksregierung Unterfranken). The mice were used with mixed sex at the age between 8 and 12 weeks. All human blood donors gave full informed consent.

Authorship contributions

J.V., C.K., S.B., M.P., I.S., M.M., J.P., M.K.S., T.P. and A.B performed experiments and analyzed data. A.S., D.S., G.S., A.B., H.S.H, K.G.H., M.S., and B.N. analyzed data from experiments, discussed results and provided scientific input throughout the study. J.V., M.P., T.V., A.B. and B.N. wrote the manuscript with input from all the authors. B.N. conceived the study, designed research.

Acknowledgements

This study was supported by the Deutsche Forschungsgemeinschaft (SFB/TR 240, project number 374031971, A07 to B.N. and M.S., B06 to K.G.H., M.S. and D.S., Z02 to A.S. and grant NI 556/11-2 to B.N.) and by the European Union (Thrombo-Inflame, EFRE–Europäischer Fonds für regionale Entwicklung, Bavaria). We thank Sylvia Hengst and Birgit Midloch for excellent technical assistance and Dr. Katharina Remer for support with documentation and management of animal experimentation and welfare. We also thank Dr. Lars Schönemann and Michelle Endres from the recombinant protein expression facility of the Rudolf Virchow Center for purification of recombinant BIN2 and STIM1. J.V. was supported by a grant of the German Excellence Initiative to the Graduate School of Life Sciences, University of Würzburg. A.S. is supported by the Ministerium für Kultur und Wissenschaft des Landes Nordrhein-Westfalen, the Regierende Bürgermeister von Berlin - inkl. Wissenschaft und Forschung, and the Bundesministerium für Bildung und Forschung.

References

1. Jackson SP. Arterial thrombosis--insidious, unpredictable and deadly. *Nat Med.* 2011;17(11):1423-36.
2. Bhatt DL. Intensifying platelet inhibition--navigating between Scylla and Charybdis. *N Engl J Med.* 2007;357(20):2078-81.
3. Jackson SP. The growing complexity of platelet aggregation. *Blood.* 2007;109(12):5087-95.
4. Stoll G, and Nieswandt B. Thrombo-inflammation in acute ischaemic stroke - implications for treatment. *Nat Rev Neurol.* 2019;15(8):473-81.
5. Stegner D, and Nieswandt B. Platelet receptor signaling in thrombus formation. *J Mol Med (Berl).* 2011;89(2):109-21.
6. Mammadova-Bach E, Nagy M, Heemskerk JWM, Nieswandt B, and Braun A. Store-operated calcium entry in thrombosis and thrombo-inflammation. *Cell Calcium.* 2019;77:39-48.
7. Grosse J, Braun A, Varga-Szabo D, Beyersdorf N, Schneider B, Zeitlmann L, et al. An EF hand mutation in Stim1 causes premature platelet activation and bleeding in mice. *J Clin Invest.* 2007;117(11):3540-50.
8. Bergmeier W, Oh-Hora M, McCarl CA, Roden RC, Bray PF, and Feske S. R93W mutation in Orai1 causes impaired calcium influx in platelets. *Blood.* 2009;113(3):675-8.
9. Varga-Szabo D, Braun A, Kleinschnitz C, Bender M, Pleines I, Pham M, et al. The calcium sensor STIM1 is an essential mediator of arterial thrombosis and ischemic brain infarction. *J Exp Med.* 2008;205(7):1583-91.
10. Braun A, Varga-Szabo D, Kleinschnitz C, Pleines I, Bender M, Austinat M, et al. Orai1 (CRACM1) is the platelet SOC channel and essential for pathological thrombus formation. *Blood.* 2009;113(9):2056-63.
11. Liou J, Kim ML, Heo WD, Jones JT, Myers JW, Ferrell JE, Jr., et al. STIM is a Ca2+ sensor essential for Ca2+-store-depletion-triggered Ca2+ influx. *Curr Biol.* 2005;15(13):1235-41.
12. Luik RM, Wu MM, Buchanan J, and Lewis RS. The elementary unit of store-operated Ca2+ entry: local activation of CRAC channels by STIM1 at ER-plasma membrane junctions. *J Cell Biol.* 2006;174(6):815-25.
13. Wu MM, Buchanan J, Luik RM, and Lewis RS. Ca2+ store depletion causes STIM1 to accumulate in ER regions closely associated with the plasma membrane. *J Cell Biol.* 2006;174(6):803-13.
14. Zhang SL, Yu Y, Roos J, Kozak JA, Deerinck TJ, Ellisman MH, et al. STIM1 is a Ca2+ sensor that activates CRAC channels and migrates from the Ca2+ store to the plasma membrane. *Nature.* 2005;437(7060):902-5.
15. Xu P, Lu J, Li Z, Yu X, Chen L, and Xu T. Aggregation of STIM1 underneath the plasma membrane induces clustering of Orai1. *Biochem Biophys Res Commun.* 2006;350(4):969-76.
16. Thillaiappan NB, Chavda AP, Tovey SC, Prole DL, and Taylor CW. Ca(2+) signals initiate at immobile IP3 receptors adjacent to ER-plasma membrane junctions. *Nat Commun.* 2017;8(1):1505.
17. Sampieri A, Santoyo K, Asanov A, and Vaca L. Association of the IP3R to STIM1 provides a reduced intraluminal calcium microenvironment, resulting in enhanced store-operated calcium entry. *Sci Rep.* 2018;8(1):13252.
18. Feng JM, Hu YK, Xie LH, Colwell CS, Shao XM, Sun XP, et al. Golli protein negatively regulates store depletion-induced calcium influx in T cells. *Immunity.* 2006;24(6):717-27.
19. Palty R, Raveh A, Kaminsky I, Meller R, and Reuveny E. SARAF inactivates the store operated calcium entry machinery to prevent excess calcium refilling. *Cell.* 2012;149(2):425-38.

20. Srikanth S, Jew M, Kim KD, Yee MK, Abramson J, and Gwack Y. Junctate is a Ca2+-sensing structural component of Orai1 and stromal interaction molecule 1 (STIM1). *Proc Natl Acad Sci U S A.* 2012;109(22):8682-7.
21. Berridge MJ, Bootman MD, and Roderick HL. Calcium signalling: dynamics, homeostasis and remodelling. *Nat Rev Mol Cell Biol.* 2003;4(7):517-29.
22. Groschner K, Shrestha N, and Fameli N. In: Kozak JA, and Putney JW, Jr. eds. *Calcium Entry Channels in Non-Excitable Cells*. Boca Raton (FL); 2018:177-96.
23. Stanishneva-Konovalova TB, Derkacheva NI, Polevova SV, and Sokolova OS. The Role of BAR Domain Proteins in the Regulation of Membrane Dynamics. *Acta Naturae.* 2016;8(4):60-9.
24. Carman PJ, and Dominguez R. BAR domain proteins-a linkage between cellular membranes, signaling pathways, and the actin cytoskeleton. *Biophys Rev.* 2018;10(6):1587-604.
25. Ren G, Vajjhala P, Lee JS, Winsor B, and Munn AL. The BAR domain proteins: molding membranes in fission, fusion, and phagy. *Microbiol Mol Biol Rev.* 2006;70(1):37-120.
26. Sakamuro D, Elliott KJ, Wechsler-Reya R, and Prendergast GC. BIN1 is a novel MYC-interacting protein with features of a tumour suppressor. *Nat Genet.* 1996;14(1):69-77.
27. Hong TT, Smyth JW, Gao D, Chu KY, Vogan JM, Fong TS, et al. BIN1 localizes the L-type calcium channel to cardiac T-tubules. *PLoS Biol.* 2010;8(2):e1000312.
28. Hong T, Yang H, Zhang SS, Cho HC, Kalashnikova M, Sun B, et al. Cardiac BIN1 folds T-tubule membrane, controlling ion flux and limiting arrhythmia. *Nat Med.* 2014;20(6):624-32.
29. Simionescu-Bankston A, Leoni G, Wang Y, Pham PP, Ramalingam A, DuHadaway JB, et al. The N-BAR domain protein, Bin3, regulates Rac1- and Cdc42-dependent processes in myogenesis. *Dev Biol.* 2013;382(1):160-71.
30. Ge K, and Prendergast GC. Bin2, a functionally nonredundant member of the BAR adaptor gene family. *Genomics.* 2000;67(2):210-20.
31. Sanchez-Barrena MJ, Vallis Y, Clatworthy MR, Doherty GJ, Veprintsev DB, Evans PR, et al. Bin2 is a membrane sculpting N-BAR protein that influences leucocyte podosomes, motility and phagocytosis. *PLoS One.* 2012;7(12):e52401.
32. Baba Y, Nishida K, Fujii Y, Hirano T, Hikida M, and Kurosaki T. Essential function for the calcium sensor STIM1 in mast cell activation and anaphylactic responses. *Nat Immunol.* 2008;9(1):81-8.
33. Gwack Y, Srikanth S, Oh-Hora M, Hogan PG, Lamperti ED, Yamashita M, et al. Hair loss and defective T- and B-cell function in mice lacking ORAI1. *Mol Cell Biol.* 2008;28(17):5209-22.
34. Munzer P, Walker-Allgaier B, Geue S, Langhauser F, Geuss E, Stegner D, et al. CK2beta regulates thrombopoiesis and Ca(2+)-triggered platelet activation in arterial thrombosis. *Blood.* 2017;130(25):2774-85.
35. van de Linde S, Loschberger A, Klein T, Heidbreder M, Wolter S, Heilemann M, et al. Direct stochastic optical reconstruction microscopy with standard fluorescent probes. *Nat Protoc.* 2011;6(7):991-1009.
36. Heilemann M, van de Linde S, Schuttpelz M, Kasper R, Seefeldt B, Mukherjee A, et al. Subdiffraction-resolution fluorescence imaging with conventional fluorescent probes. *Angew Chem Int Ed Engl.* 2008;47(33):6172-6.
37. Weber K, Rathke PC, and Osborn M. Cytoplasmic microtubular images in glutaraldehyde-fixed tissue culture cells by electron microscopy and by immunofluorescence microscopy. *Proc Natl Acad Sci U S A.* 1978;75(4):1820-4.
38. Durrant TN, van den Bosch MT, and Hers I. Integrin alphaIIbbeta3 outside-in signaling. *Blood.* 2017;130(14):1607-19.
39. Gilio K, van Kruchten R, Braun A, Berna-Erro A, Feijge MA, Stegner D, et al. Roles of platelet STIM1 and Orai1 in glycoprotein VI- and thrombin-dependent procoagulant activity and thrombus formation. *J Biol Chem.* 2010;285(31):23629-38.

40. Gruner S, Prostredna M, Aktas B, Moers A, Schulte V, Krieg T, et al. Anti-glycoprotein VI treatment severely compromises hemostasis in mice with reduced alpha2beta1 levels or concomitant aspirin therapy. *Circulation.* 2004;110(18):2946-51.
41. Inoue O, Suzuki-Inoue K, Dean WL, Frampton J, and Watson SP. Integrin alpha2beta1 mediates outside-in regulation of platelet spreading on collagen through activation of Src kinases and PLCgamma2. *J Cell Biol.* 2003;160(5):769-80.
42. Dutting S, Vogtle T, Morowski M, Schiessl S, Schafer CM, Watson SK, et al. Growth factor receptor-bound protein 2 contributes to (hem)immunoreceptor tyrosine-based activation motif-mediated signaling in platelets. *Circ Res.* 2014;114(3):444-53.
43. Cherpokova D, Bender M, Morowski M, Kraft P, Schuhmann MK, Akbar SM, et al. SLAP/SLAP2 prevent excessive platelet (hem)ITAM signaling in thrombosis and ischemic stroke in mice. *Blood.* 2015;125(1):185-94.
44. Dong M, Zheng N, Ren LJ, Zhou H, and Liu J. Increased expression of STIM1/Orai1 in platelets of stroke patients predictive of poor outcomes. *Eur J Neurol.* 2017;24(7):912-9.
45. Kleinschnitz C, Pozgajova M, Pham M, Bendszus M, Nieswandt B, and Stoll G. Targeting platelets in acute experimental stroke: impact of glycoprotein Ib, VI, and IIb/IIIa blockade on infarct size, functional outcome, and intracranial bleeding. *Circulation.* 2007;115(17):2323-30.
46. Boulay G, Brown DM, Qin N, Jiang M, Dietrich A, Zhu MX, et al. Modulation of Ca(2+) entry by polypeptides of the inositol 1,4, 5-trisphosphate receptor (IP3R) that bind transient receptor potential (TRP): evidence for roles of TRP and IP3R in store depletion-activated Ca(2+) entry. *Proc Natl Acad Sci U S A.* 1999;96(26):14955-60.
47. Beliveau E, Lessard V, and Guillemette G. STIM1 positively regulates the Ca2+ release activity of the inositol 1,4,5-trisphosphate receptor in bovine aortic endothelial cells. *PLoS One.* 2014;9(12):e114718.
48. Patterson RL, Boehning D, and Snyder SH. Inositol 1,4,5-trisphosphate receptors as signal integrators. *Annu Rev Biochem.* 2004;73:437-65.
49. Prole DL, and Taylor CW. Inositol 1,4,5-trisphosphate receptors and their protein partners as signalling hubs. *J Physiol.* 2016;594(11):2849-66.
50. Malkusch S, Endesfelder U, Mondry J, Gelleri M, Verveer PJ, and Heilemann M. Coordinate-based colocalization analysis of single-molecule localization microscopy data. *Histochem Cell Biol.* 2012;137(1):1-10.
51. Ambily A, Kaiser WJ, Pierro C, Chamberlain EV, Li Z, Jones CI, et al. The role of plasma membrane STIM1 and Ca(2+)entry in platelet aggregation. STIM1 binds to novel proteins in human platelets. *Cell Signal.* 2014;26(3):502-11.
52. Feske S. CRAC channels and disease - From human CRAC channelopathies and animal models to novel drugs. *Cell Calcium.* 2019;80:112-6.
53. Schwenk F, Baron U, and Rajewsky K. A cre-transgenic mouse strain for the ubiquitous deletion of loxP-flanked gene segments including deletion in germ cells. *Nucleic Acids Res.* 1995;23(24):5080-1.
54. Tiedt R, Schomber T, Hao-Shen H, and Skoda RC. Pf4-Cre transgenic mice allow the generation of lineage-restricted gene knockouts for studying megakaryocyte and platelet function in vivo. *Blood.* 2007;109(4):1503-6.
55. Winkler C, Denker K, Wortelkamp S, and Sickmann A. Silver- and Coomassie-staining protocols: detection limits and compatibility with ESI MS. *Electrophoresis.* 2007;28(12):2095-9.
56. Premsler T, Lewandrowski U, Sickmann A, and Zahedi RP. Phosphoproteome analysis of the platelet plasma membrane. *Methods Mol Biol.* 2011;728:279-90.
57. Stritt S, Nurden P, Turro E, Greene D, Jansen SB, Westbury SK, et al. A gain-of-function variant in DIAPH1 causes dominant macrothrombocytopenia and hearing loss. *Blood.* 2016;127(23):2903-14.

58. Stritt S, Birkholz I, Beck S, Sorrentino S, Sapra KT, Viaud J, et al. Profilin 1-mediated cytoskeletal rearrangements regulate integrin function in mouse platelets. *Blood Adv.* 2018;2(9):1040-5.
59. Aurbach K, Spindler M, Haining EJ, Bender M, and Pleines I. Blood collection, platelet isolation and measurement of platelet count and size in mice-a practical guide. *Platelets.* 2018:1-10.
60. Pleines I, Eckly A, Elvers M, Hagedorn I, Eliautou S, Bender M, et al. Multiple alterations of platelet functions dominated by increased secretion in mice lacking Cdc42 in platelets. *Blood.* 2010;115(16):3364-73.
61. Heemskerk JW, Feijge MA, Rietman E, and Hornstra G. Rat platelets are deficient in internal Ca2+ release and require influx of extracellular Ca2+ for activation. *FEBS Lett.* 1991;284(2):223-6.
62. Schuhmann MK, Kraft P, Stoll G, Lorenz K, Meuth SG, Wiendl H, et al. CD28 superagonist-mediated boost of regulatory T cells increases thrombo-inflammation and ischemic neurodegeneration during the acute phase of experimental stroke. *J Cereb Blood Flow Metab.* 2015;35(1):6-10.
63. Richter KN, Revelo NH, Seitz KJ, Helm MS, Sarkar D, Saleeb RS, et al. Glyoxal as an alternative fixative to formaldehyde in immunostaining and super-resolution microscopy. *EMBO J.* 2018;37(1):139-59.
64. Nieswandt B, Bergmeier W, Rackebrandt K, Gessner JE, and Zirngibl H. Identification of critical antigen-specific mechanisms in the development of immune thrombocytopenic purpura in mice. *Blood.* 2000;96(7):2520-7.
65. Wolter S, Loschberger A, Holm T, Aufmkolk S, Dabauvalle MC, van de Linde S, et al. rapidSTORM: accurate, fast open-source software for localization microscopy. *Nat Methods.* 2012;9(11):1040-1.

Figure 1

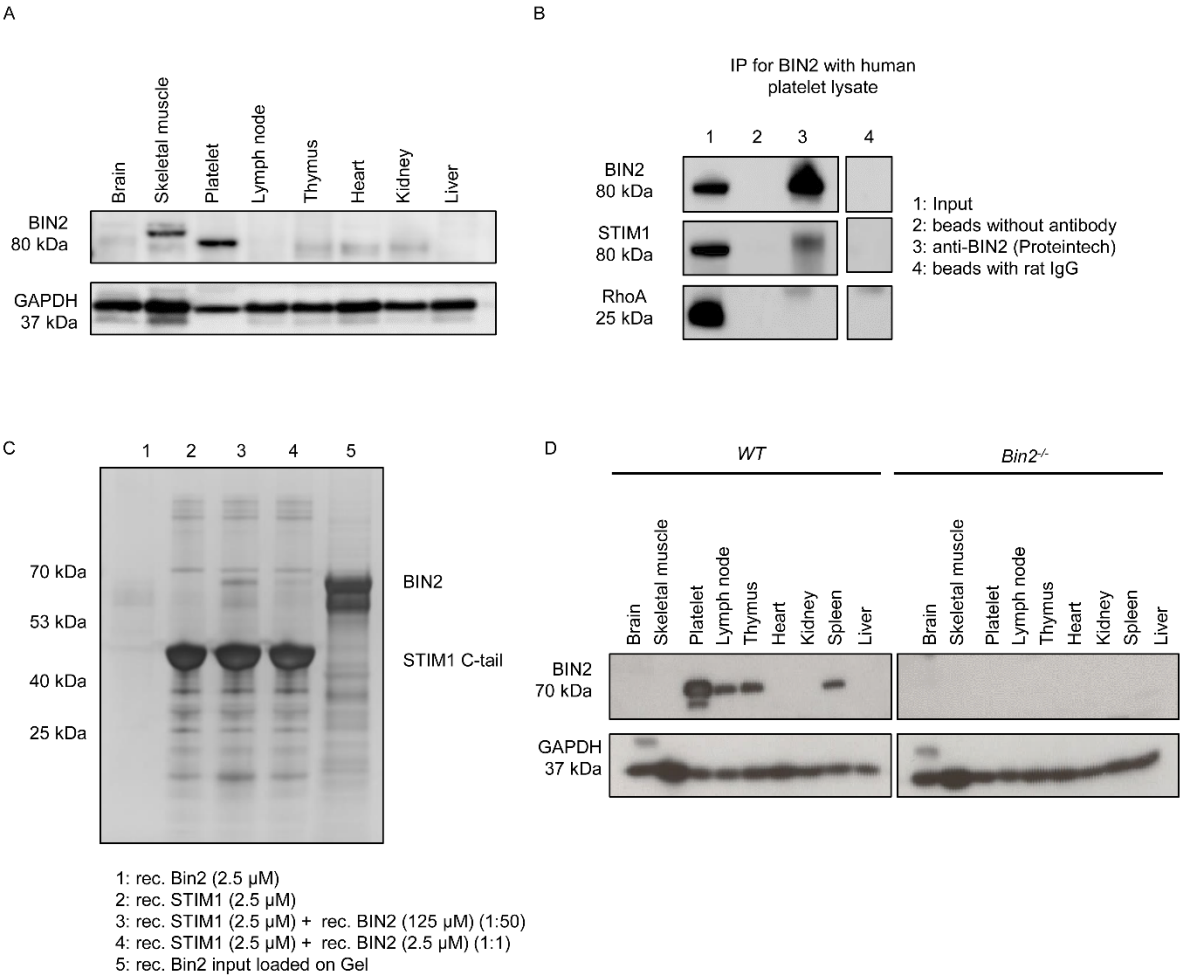

Figure 1: BIN2 is highly expressed in human and mouse platelets

(A) Western blot analysis of BIN2 expression in human tissue lysates, GAPDH was used as loading control. **(B)** Immunoprecipitation of BIN2 was perfomed with human platelet lysates using an anti-BIN2 antibody (Proteintech). BIN2, STIM1 and RhoA were detected by Western Blot. Representative result of three independent experiments. Lane 4 was run on the same gel as 1-3 but the lanes were noncontiguous. **(C)** Recombinant GST-tagged STIM1 C-tail incubated with recombinant BIN2 protein. Pulldown of the GST-tagged STIM1 was performed and the resulting fractions were analysed by SDS page and silver staining. **(D)** Western blot analysis of BIN2 expression in the indicated tissue lysates of *WT* and *Bin2*$^{-/-}$ mice with GAPDH as loading control.

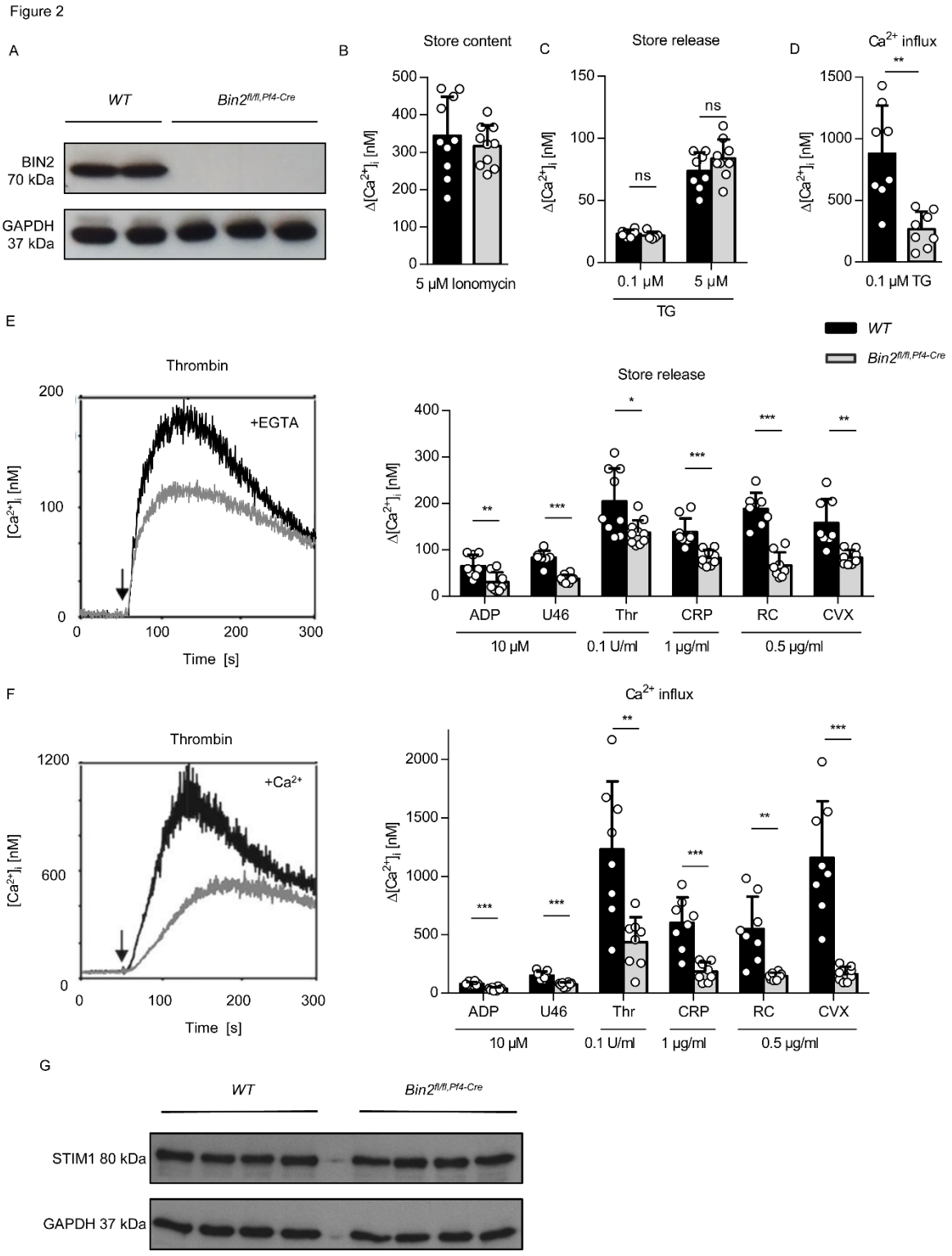

Figure 2: Impaired Ca^{2+} store release and influx in *Bin2*$^{fl/fl,Pf4Cre}$ platelets

(A) Western blot analysis of BIN2 expression in *WT* and *Bin2*$^{fl/fl,Pf4Cre}$ platelet lysates with GAPDH as loading control. **(B)** Ca^{2+} store content was measured upon stimulation with 5 µM ionomycin in the presence of 0.5 mM EGTA (n=10) **(C)** Ca^{2+} store release was measured in the absence of extracellular Ca^{2+} upon treatment with 0.1 µM or 5 µM thapsigargin (TG) (n≥8) and **(D)** Ca^{2+} influx upon treatment with 0.1 µM TG (n=8) **(E, F)** Representative traces and statistical analysis of store release (E) and Ca^{2+} influx (F) upon activation of the platelets with the indicated agonists (n≥8) **(G)** Western blot analysis of WT and *Bin2*$^{fl/fl,Pf4Cre}$ platelet lysates

detecting the expression of STIM1 with GAPDH as a loading control. Values are depicted as mean ± SD and P-values were calculated using the Mann-Whitney test. *P<0.05, **P<0.01, ***P<0.001

Figure 3

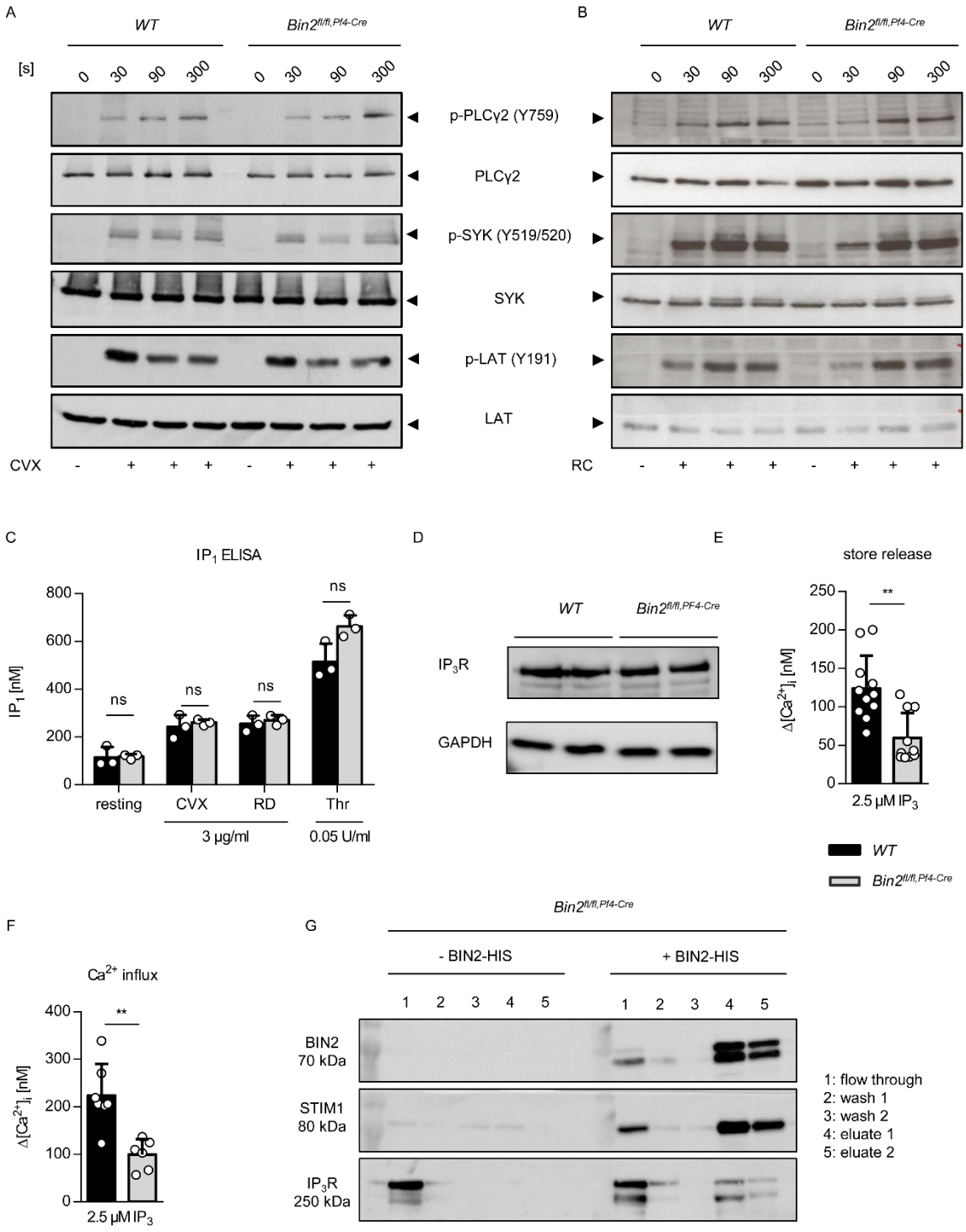

Figure 3: Defective IP_3R function in *Bin2$^{fl/fl,Pf4Cre}$* mice and BIN2 interaction with STIM1 and IP_3R

(A, B) Determination of whole cell tyrosine phosphorylation pattern in *WT* and *Bin2$^{fl/fl,Pf4Cre}$* platelets upon activation with convulxin (CVX) (A) or rhodocytin (RC) (B). The samples were taken at the indicated time points, lysed and Western blot analysis was performed with the indicated phosphospecific and pan-antibodies. This blot is representative of three independent experiments. **(C)** Quantification of inositol monophosphate (IP1), a specific metabolite of inositol-1,4,5-trisphosphate (IP3), produced upon activation with the indicated agonist (n=3).

Representative results of three independent experiments. **(D)** Western blot analysis of IP_3R expression in *WT* and *Bin2*$^{fl/fl,Pf4Cre}$ platelet lysates; GAPDH was used as loading control. **(E, F)** Ca^{2+} concentrations in the cytoplasm of *WT* and *Bin2*$^{fl/fl,Pf4Cre}$ platelets upon treatment with UV light inducible IP_3 in the (E) absence or (F) presence of extracellular Ca^{2+} (n=8) **(G)** *Bin2*$^{fl/fl,Pf4Cre}$ platelet lysates were incubated with recombinant BIN2-HIS protein, followed by a purification step with NI-NTA beads. The different fractions were eluted and analyzed by Western blotting using BIN2-, STIM1- and IP_3R-specific antibodies. Representative result of three independent experiments. Values are depicted as mean ± SD and P-values were calculated using the Mann-Whitney test. **P<0.01

Figure 4

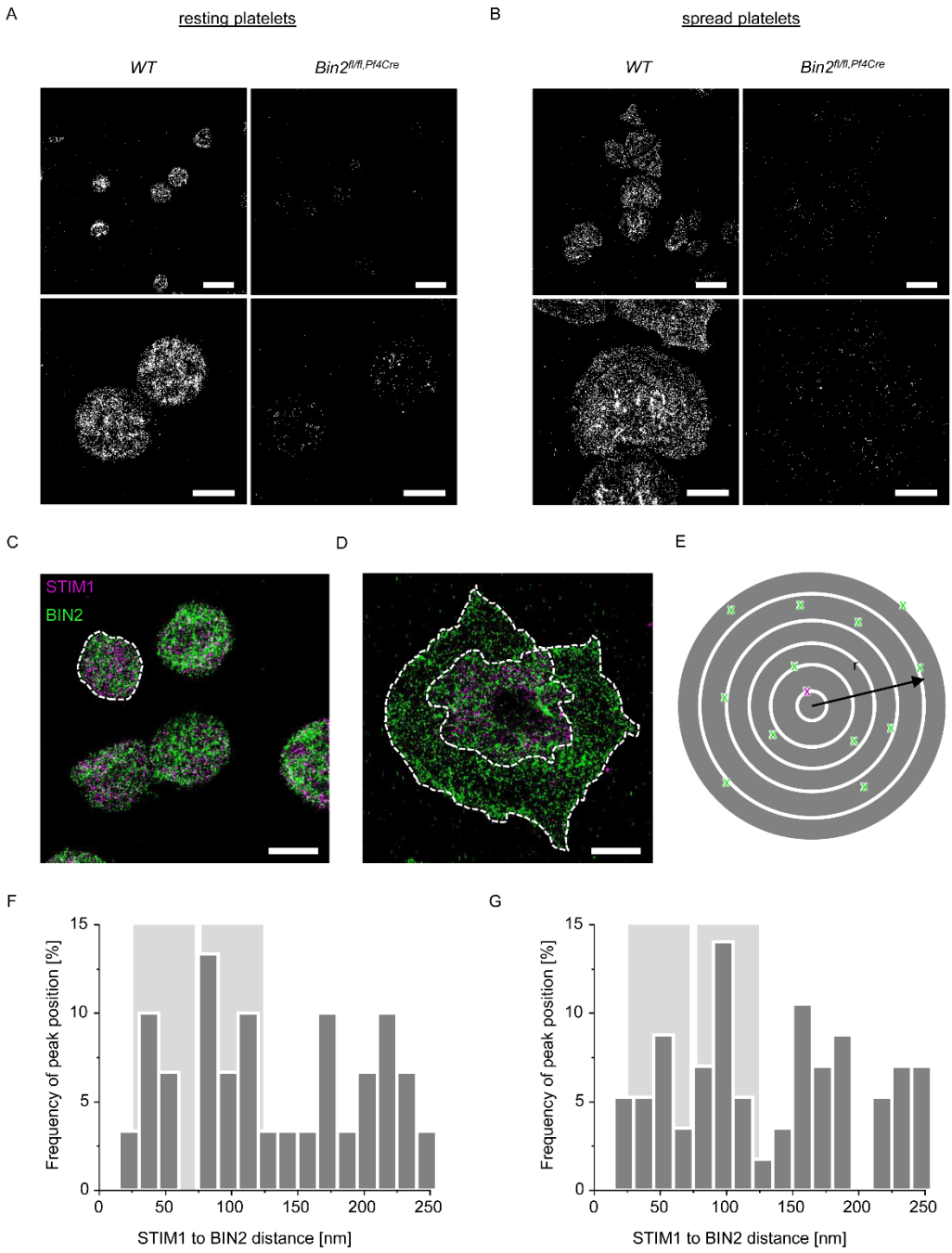

Figure 4: BIN2 STIM1 co-localization in human platelets

*d*STORM images of **(A)** resting mouse platelets on glycine or **(B)** thrombin activated *WT* and *Bin2*$^{fl/fl,Pf4Cre}$ mouse platelets on fibrinogen, stained for BIN2. Scale bar upper panel: 5 µm, lower panel: 2 µm. Dual-color *d*STORM allows to resolve the distribution of STIM1 (magenta) and BIN2 (green) in **(C)** resting and **(D)** activated human platelets; dashed white lines indicate areas of neighbor density analysis **(E)** between STIM1 (magenta) and BIN2 (green) with discrete ring areas in which the BIN2 density was determined (dark gray). In activated spread platelets, only localizations in the inner region where the organelles and intercellular membrane compartments accumulate were considered for STIM1. Colocalization hotspots of STIM1 and BIN2 are identified by analyzing the BIN2 density at increasing radial distances to

STIM1: Histograms of the distance dependent BIN2 density peak maxima found for **(F)** resting (n=6, Suppl. Figure 7A) and **(G)** activated human platelets (n=14, Suppl. Figure 7B). The distinct STIM1 to BIN2 distance regions with increased accumulation of co-localization hotspots are highlighted in light gray. Scale bars **(C,D):** 2 µm.

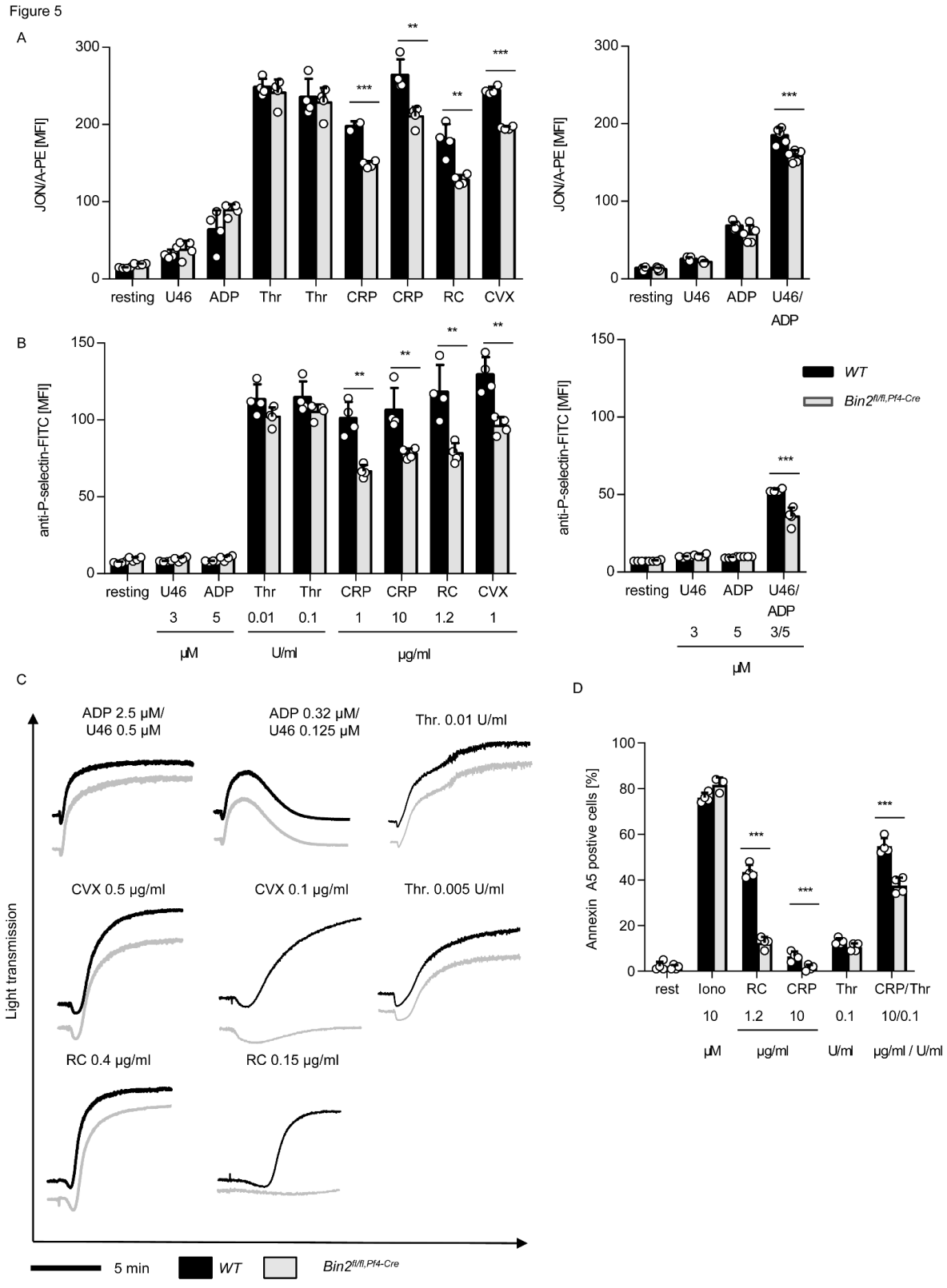

Figure 5: Defective integrin activation and aggregation of *Bin2*$^{fl/fl,Pf4Cre}$ platelets upon (hem)ITAM stimulation

(A, B) Flow cytometric analysis of (A) integrin αIIbβ3 activation (binding of JON/A-PE) and (B) degranulation-dependent P-selectin exposure in *WT* and *Bin2*$^{fl/fl,Pf4Cre}$ platelets in response to the indicated agonists (n=4). Representative result of three independent experiments. Values are depicted as mean ± SD and P-values were calculated using the Mann-Whitney test.

P<0.01, ***P<0.001 **(C) Washed platelets were stimulated with the indicated agonists, and light transmission was recorded using a four channel aggregometer. Representative results of three independent experiments. (D) Phoshpatidyserine exposure of platelets in response to the indicated agonists was measured by flow cytometry. n≥5. Representative result of three independent experiments. Values are depicted as mean ± SD and P-values were calculated using the Mann-Whitney test. **P<0.01, ***P<0.001

Figure 6

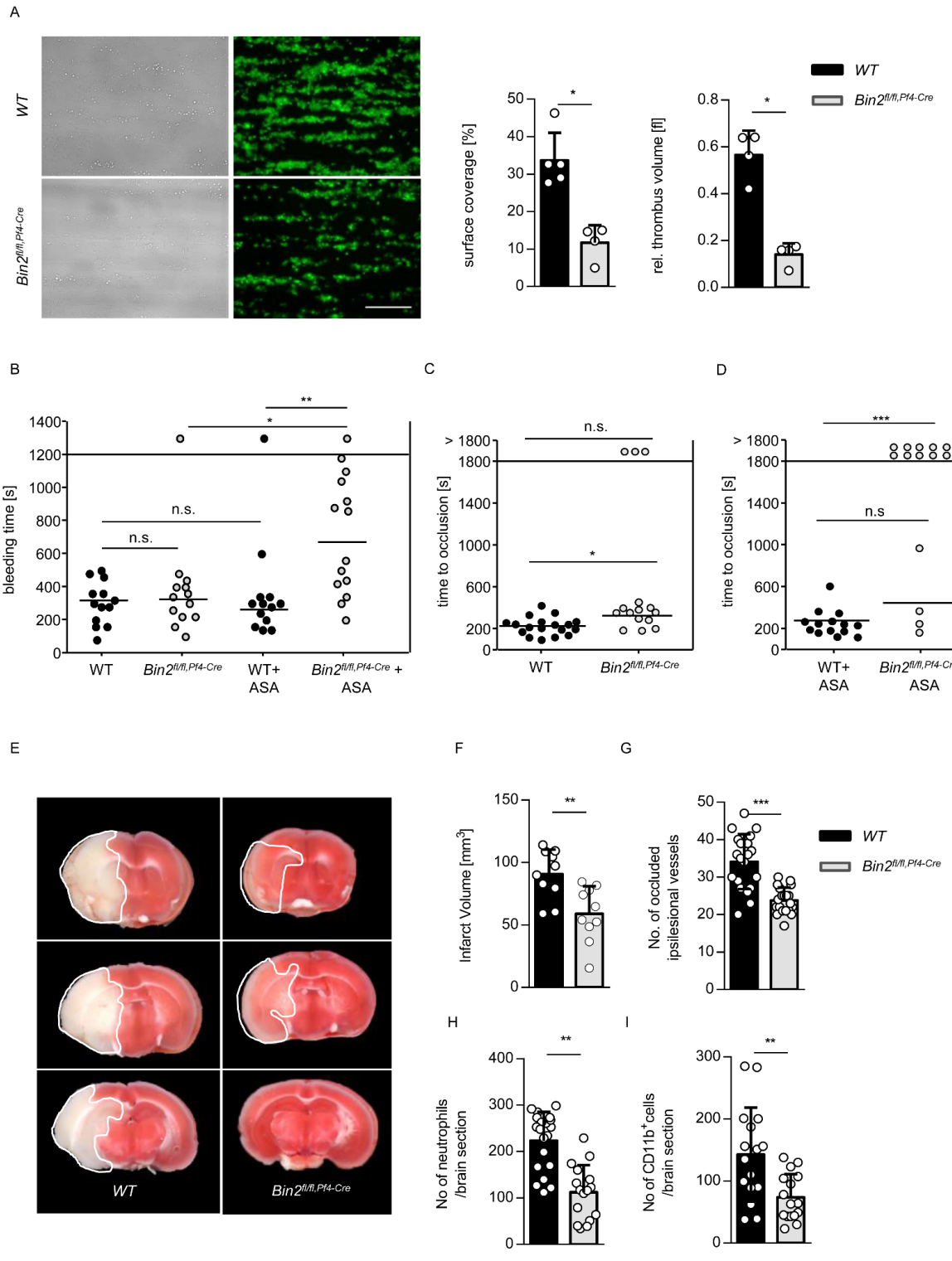

Figure 6: Impaired hemostasis, defective arterial thrombus formation and protection from ischemic brain infarction in *Bin2*$^{fl/fl,Pf4Cre}$ mice

(A) Adhesion and thrombus formation of platelets on collagen was assessed in a flow adhesion assay at a wall shear rate of 1700 s^{-1}. Representative images and the quantification of the surface coverage and the relative thrombus volume are shown (n=4). Representative example of three independent experiments. Values are depicted as mean ± SD and P-values were

calculated using the Mann-Whitney test. *P<0.05. Scale bar: 50 µm **(B)** Tail bleeding times of *WT* and *Bin2*$^{fl/fl,Pf4Cre}$ mice with or without acetylsalicylic acid (ASA) treatment (1 mg/kg i.v.) 15 minutes before the start of the experiment. Each symbol represents 1 animal. Kruskal-Wallis test (p-value: 0.0022) followed by Dunn's multiple comparisons post-hoc test; *P<0.05, **P<0.01 **(C;D)** Time to stable vessel occlusion of *WT* and *Bin2*$^{fl/fl,Pf4Cre}$ mice withthout (C) or with (D) ASA treatment (1 mg/kg i.v.) 15 minutes before the start of the experiment. The abdominal aorta was injured by firm compression with a forceps, and blood flow was monitored for 30 minutes. Mann-Whitney U test was performed to compare mean occlusion times of occluded vessels. To compare frequency of occluded and non-occluded vessels, Fisher's exact test was used. *P<0.05, ***P<0.001 **(E-I)** *WT* and Bin2$^{fl/fl\ Pf4\text{-}Cre}$ mice were subjected to 60 minutes of transient middle cerebral artery occlusion (tMCAO) n=10. (E) Representative images of 3 coronal brain sections stained with 2,3,5-triphenyltetrazolium chloride. (F) Infarct volumes, (G) number of occluded ipsilateral vessels, (two slides per animal analysed) (H) number of neutrophils and (I) $CD11b^+$ cells per section (two slides per animal analysed) were investigated after 24 h. Values are depicted as mean ± SD and P-values were calculated using the Mann-Whitney test. **P<0.01, ***P<0.001.